Acta Cryst. (1996). A52, 730–747

Diffraction-Line Broadening due to Strain Fields in Materials; Fundamental Aspects and Methods of Analysis†

J. G. M. VAN BERKUM,‡ R. DELHEZ, TH. H. DE KEIJSER AND E. J. MITTEMEIJER*

Laboratory of Materials Science, Delft University of Technology, Rotterdamseweg 137, 2628 AL Delft, The Netherlands. E-mail: mittemeijer@stm.tudelft.nl

(Received 19 May 1994; accepted 27 April 1996)

Abstract

Broadening of (X-ray) diffraction lines is often due to the distortion fields associated with lattice defects as dislocations. A generally applicable flexible model for distributions of lattice defects and their distortion fields is presented. The model allows a straightforward calculation of diffraction-line profiles. Parameters of the model are the average distance between the defects, the extent of the distortion fields and the mean-squared strain. The order dependence of the shape and width of line profiles is studied as a function of these model parameters. The adequacy for practical application of two methods frequently used to analyse X-ray diffraction-line broadening (the Warren–Averbach analysis and the Williamson–Hall analysis) is investigated by applying them to calculating line profiles. The 'size' and 'strain' parameters deduced by the methods mentioned are discussed with reference to the strain-field model parameters. It is concluded that only in limiting cases can the results be related directly to the microstructure. Experimental line profiles taken from a ball-milled tungsten powder are used to show that the line profiles calculated on the basis of the strain-field model pertain to realistic situations. It is shown that, in principle, an interpretation of measured line broadening is possible directly in terms of strain-field parameters.

1. Introduction

Broadening of (X-ray) diffraction-line profiles is caused by non-ideal optics of the instrument, wavelength dispersion and structural imperfectness of the specimen. In the generally adopted theories (*e.g.* Warren, 1969; Wilson, 1970), two kinds of structural line broadening are distinguished that can occur simultaneously: (i) size broadening, caused by a finite size of regions in the specimen diffracting incoherently§ with respect to each other; and (ii) strain broadening, due to varying displacements of the atoms with respect to their reference positions. Size broadening is independent of the order of reflection and strain broadening is order dependent.

For the application of the theories mentioned above, it is essential to understand when parts of a specimen can be considered to diffract incoherently. In general, the whole irradiated volume of a (polycrystalline) specimen can be considered as a single coherently diffracting unit because in reality the diffracted intensity is determined by the interference of all waves scattered in the specimen§ (even if they come from different crystals or grains). Thus, in principle, line broadening always comprises a size-broadening component reflecting the size of the *specimen* (even for polycrystalline specimens) and a (strain) broadening component reflecting the relative displacements of all atoms *in the whole specimen*. In many cases, the latter broadening component can be subdivided further. Normally, the specimen-size broadening is very small and it will be ignored here.

For most polycrystalline specimens, the relative position and orientation of the grains is so variable and the number of grains is so large that the phase differences (reduced modulo 2π) between a wave scattered by one grain and waves scattered by other grains take all values between 0 and 2π with equal probability. The intensity scattered by the assembly of grains then equals the sum of the intensities scattered by the grains separately, *i.e.* the grains diffract incoherently (*e.g.* Sommerfeld, 1964; Fowles, 1968). In such a case, the line broadening can (also) be considered to consist of a size-broadening component reflecting the size of the *grains* and a (strain) broadening component reflecting only the relative displacements of the atoms *within the same grain*.

For many polycrystalline specimens, the grain-size broadening is negligible. It has been argued that owing to the presence of certain lattice defects even parts ('domains') of grains can be considered to diffract

† Appendices written by J. G. M. van Berkum.

‡ Present address: Philips Research Laboratories, Prof. Holstlaan 4 (WY-42), 5656 AA Eindhoven, The Netherlands.

§ Instead of 'independently diffracting or scattering', the expression 'incoherently diffracting' is used throughout this paper because it has been used in former discussions (*e.g.* Warren, 1959).

§ The limited coherency of the incident radiation in the directions parallel and perpendicular to the direction of wave propagation [usually $\sim 1\mu m$ and a few tens of nm, respectively, for X-rays (Cowley, 1981)] is ignored in this paper.

incoherently. This would imply that the line broadening can (also) be considered as the combination of a size-broadening component reflecting the size of the *domains* and a strain broadening component reflecting only the relative displacements of the atoms *within the same domain*. However, it has never been shown under which conditions which lattice defects can cause incoherently diffracting domains. This is the first problem addressed in the present paper (§3).

This first problem is investigated by calculating line profiles on the basis of a generally applicable flexible model for the strain field in a deformed grain. The model represents the distribution of lattice defects, which distort the surrounding material (§2). The line broadening is calculated rigorously without assuming that parts of the grain diffract incoherently, *i.e.* the interference (phase differences) of all waves scattered in the grain is taken into account. From the order-dependence of the calculated line-profile characteristics, it can be concluded by hindsight if parts of the modelled grain could also have been considered to diffract incoherently; *i.e.* if order-independent '(domain) size' broadening occurs (§3).

The second aim of this paper is to investigate the meaning of the 'size' and 'strain' values obtained by means of current line-profile decomposition methods (§4). These methods of line-broadening analysis use measured line profiles of two or more orders of reflection and try to decompose these into an order-independent size part and an order-dependent strain part on the basis of assumptions about the order dependence of strain broadening. In many applications (*e.g.* to cold-worked metals), a significant size-broadening contribution, much larger than expected on the basis of the grain size, is found. Such results may be erroneous if the assumptions used were inappropriate for the specimen under study or they may be an indication of the presence of lattice defects with strain fields that give rise to almost order-independent strain broadening (interpreted as domain broadening, see above). This second problem is investigated by using line profiles calculated on the basis of the strain-field model (§4) and line profiles measured from a cold-worked specimen (§6.1).

Since one of the line-profile decomposition methods, the Warren–Averbach analysis, has been the subject of many previous discussions, a few comments on this method in advance may be helpful. The line-broadening *theory* developed by Warren & Averbach (1950) is generally accepted. Also, their *analysis* (Warren & Averbach, 1952), developed on the basis of this theory, to extract the 'size' and the (local) mean-squared strain is correct in principle. The analysis assumes small even moments of the strain distributions or approximately Gaussian strain distributions (Warren & Averbach, 1952; see also van Berkum, Vermeulen, Delhez, de Keijser & Mittemeijer, 1994) and it requires determination of the initial slope of the size Fourier coefficient curve. This usually poses problems in practice. As a result, the size and strain parameters obtained from Warren–Averbach analyses, as presented in publications, may be biased to an unknown extent [see compilation of data in Klug & Alexander (1974) and discussion in van Berkum, Vermeulen, Delhez, de Keijser & Mittemeijer (1994)].

The third aim of this paper is to investigate the usefulness of line-profile simulation on the basis of the strain-field model presented in §2 for an interpretation of experimental line broadening (§5 and §6) by matching simulation to experiment (see also van Berkum, Delhez, de Keijser & Mittemeijer, 1992). The line-profile simulation itself involves no assumptions on order-independent or order-dependent contributions to the line broadening. Therefore, if adequate strain models can be developed, this approach can be valuable in diffraction-line broadening analysis.

2. Model

A line profile $I(2\theta)$, measured as a function of the diffraction angle 2θ, corresponds to a profile $I'(s, d^*)$ in reciprocal space with $s = [2\sin\theta/\lambda] - d^*$, where λ is the wavelength of the radiation used and where d^* corresponds to the centroid of $I'(s, d^*)$. The profile $I'(s, d^*)$ can be expressed as a Fourier series:†

$$I'(s, d^*) = K \sum_{L=-\infty}^{+\infty} [A(L, d^*)\cos(2\pi Ls) + B(L, d^*)\sin(2\pi Ls)], \quad (1)$$

where K is (approximately) a constant, A and B are the cosine and sine Fourier coefficients and L is called the 'correlation length', a distance in real space parallel to the diffraction vector $\mathbf{H}$ (*i.e.* perpendicular to the diffracting planes). In practice, L is considered as a continuous variable. Within the kinematical diffraction theory, the Fourier coefficients of a line profile broadened by lattice distortions can be written as (Warren, 1959, 1969):

$$A(L, d^*) = \langle\cos(2\pi d^* Z_L)\rangle = \int_{-\infty}^{\infty} p_{Z_L}(Z_L)\cos(2\pi d^* Z_L)\,\mathrm{d}Z_L \quad (2)$$

$$B(L, d^*) = \langle\sin(2\pi d^* Z_L)\rangle = \int_{-\infty}^{\infty} p_{Z_L}(Z_L)\sin(2\pi d^* Z_L)\,\mathrm{d}Z_L, \quad (3)$$

where Z_L is the elongation that a length L parallel to $\mathbf{H}$ experiences owing to the presence of lattice distor-

† In textbooks (*e.g.* Warren, 1969), often a (fictitious) unit-cell dimension a_3 in the direction of the diffraction vector is chosen and the dimensionless quantities $n = L/a_3$, $l = d^* a_3$ and $h_3 = (d^* + s)a_3$ are used.

tions, $p_{Z_L}(Z_L)$ is the probability density function of Z_L in the diffracting volume of the specimen and $\langle \ldots \rangle$ denotes averaging over the whole diffracting volume. The factor accounting for the size broadening owing to the grain size is omitted in (2) and (3), *i.e.* the grain size is taken as infinite. A grain-size effect would obscure the effect to be investigated here (as mentioned in §1, line broadening is calculated by considering the grain as a single coherently diffracting unit; it can then be established afterwards if the grain could also have been considered as an assembly of domains scattering incoherently with respect to each other). If necessary, *e.g.* for a fine-grained material, the effect of a finite grain size can easily be included in the line-broadening calculation.

A specimen usually contains many diffracting crystals, each containing many lattice defects with associated distortion fields. Therefore, the strains in such a specimen can only be described efficiently in a statistical way. Here, statistical formulations that are considered reasonable for practice are used to describe the strain along an axis **x** parallel to **H** (see Fig. 1) and to calculate the corresponding $p_{Z_L}(Z_L)$. By substitution of $p_{Z_L}(Z_L)$ in (2) and (3), the Fourier coefficients and thereby the line profile itself are obtained. If the lattice-defect positions and their strain-field contributions are determined by a stochastic process, one observes the same probability density $p_{Z_L}(Z_L)$ along any line parallel to **x**. Then, a single infinitely long column along **x** is considered representative for all columns making up a complete three-dimensional specimen. The coordinate x along **x** is considered as a continuous variable. The elongation $Z_L(x)$ of the correlation length L can be calculated from the strain component e_{xx} parallel to **x** [in the following, e_{xx} is denoted as e; strain components other than e_{xx} do not affect $Z_L(x)$]:

$$Z_L(x) = \int_{x-L/2}^{x+L/2} e(x')\,\mathrm{d}x'. \tag{4}$$

On the axis **x**, a number of positions x_i (i is an integer) occur at which contributions to the strain field $e(x)$ along **x** are centred. These positions can be considered as the 'projections' of (point, line or planar) lattice defects close to the axis **x** (see Fig. 1). The distances between two successive projected defects $D_i = x_i - x_{i-1}$ are considered independent stochastic variables. For all variables D_i, the probability density of $D_i = D$ is given by a function $p_D(D)$ with a mean $\langle D \rangle$.

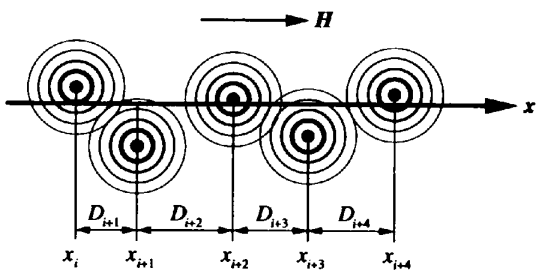

Fig. 1. Crystal defects with associated distortion fields projected onto an axis **x** parallel to the diffraction vector **H**. The projected-defect distances $D_i = x_i - x_{i-1}$ are indicated.

The meaning of the mean projected-defect distance $\langle D \rangle$ for a given three-dimensional spatial distribution of lattice defects depends on the character of the defect. In the case of planar defects, the axis **x** intersects the defects and the meaning of $\langle D \rangle$ is straightforward. In the case of linear defects (ρ defects per unit area) or point defects (c defects per unit volume), the defects that are relatively far from **x** (*e.g.* at distances larger than the average defect distance in space, $\rho^{-1/2}$ or $c^{-1/3}$, respectively) do not contribute to $e(x)$ significantly because their strain fields are shielded by others closer to **x**. For a planar section containing **x**, in a region bounded by lines parallel to **x** at distances (a few times) $\rho^{-1/2}$ from **x**, there are about (a few times) $2\rho^{1/2}$ linear defects per unit length along **x**, so that $\langle D \rangle$ is (a few times smaller than) $\frac{1}{2}\rho^{-1/2}$ for linear defects. In a cylinder around **x** with a radius (a few times) $c^{-1/3}$, there are about (a few times) $\pi c^{1/3}$ point defects per unit length along **x**, so that $\langle D \rangle$ is (a few times smaller than) $(1/\pi)c^{-1/3}$ for point defects. Thus, the average projected-defect distance $\langle D \rangle$ is, according to these examples, smaller than the average defect distance in space (here, $\rho^{-1/2}$ or $c^{-1/3}$, respectively). If the spatial distribution of the defects is not isotropic, *i.e.* different in the directions parallel and perpendicular to **H**, this interpretation should be adapted accordingly.

The total strain field $e(x)$ is written as the sum of 'component' strain fields of individual projected defects $e_i(x)$:

$$e(x) = \sum_{i=-\infty}^{\infty} e_i(x). \tag{5}$$

Each component $e_i(x)$ is written as the product of a dimensionless amplitude a_i, different for each projected defect, and a dimensionless normalized [*cf.* (29)] 'spreading' function $f(x - x_i)$, which is, apart from the location x_i, taken equal for all projected defects:

$$e_i(x) = a_i f(x - x_i). \tag{6}$$

In reality, the shape and width of the component strain field may be different for each projected defect (*e.g.* depending on the distance from the defect to the axis **x** and/or on the orientation with respect to **x**). In practice, (6) may already provide a satisfactory description of measured line broadening (see §6) and then $f(x)$ represents the 'average' shape and width of the component strain fields. The amplitudes a_i are considered independent stochastic variables. For all a_i, the probability density of $a_i = a$ is given by a function $p_a(a)$. Since the centroid of the line profile $I'(s, d^*)$ is taken as its origin, the average strain is nil (Wagner, 1966), which implies $\langle a \rangle = 0$.

In Appendix *A*, it is shown how the Fourier coefficients $A(L, d^*)$ and $B(L, d^*)$ can be calculated from (2) through (6) for arbitrary functions $p_a(a)$, $p_D(D)$ and $f(x)$. In this paper, for $p_a(a)$, $p_D(D)$ and $f(x)$, three specific functions are used.

For $p_a(a)$, a Gaussian with $\langle a^2 \rangle$ as the only parameter is considered. Since such a $p_a(a)$ is symmetrical with respect to $a = 0$, the calculated structurally broadened line profiles are symmetrical [see above (26); this implies that the sine Fourier coefficients are nil]. The use of a Gaussian $p_a(a)$ does not imply that $p_{Z_L}(Z_L)$ and the associated strain distribution are Gaussian. The shape of $p_{Z_L}(Z_L)$ depends not only on the shape of $p_a(a)$ but also on L and on the functions $f(x)$ and $p_D(D)$.

For the projected-defect distance probability density $p_D(D)$, a δ function at $D = \langle D \rangle$ [see Appendix *A*(iii)] is considered in this paper, implying equidistant projected defects: $x_i - x_{i-1} = \langle D \rangle$ for all i. For a non-periodic distribution of defects, see van Berkum *et al.* (1994), where it has also been shown that the order dependence of line broadening can be discussed on the basis of a periodic distribution of defects. Note that 'periodically distributed' defects do not imply a periodic strain field $e(x)$ because the amplitudes a_i are independent stochastic variables (*cf.* Fig. 2). Therefore, the range of meaningful Fourier coefficients in the present model is not necessarily limited to small L, as is the case with models employing periodic boundary conditions (*e.g.* Wilkens, 1979).

If the lattice defects are screw dislocations, $f(x)$ is a Lorentzian with a width depending on the distance between the axis **x** and the dislocation line (see Appendix *B*). For edge dislocations, the tails of $f(x)$ show a similar behaviour in a direction parallel to Burgers' vector (see Appendix *B*). From a comparison of $A(L, d^*)$ behaviours calculated using a Lorentzian shape and using other shapes for $f(x)$ [*e.g.* $f(x) \propto \exp(-|x|)$, which occurs on crossing a pure tilt boundary at right angles (Hirth & Lothe, 1982)], it appeared that the shape of $f(x)$ is not critical. In the following, a Lorentzian $f(x)$ with w as the half-width at half-height is used. Examples of behaviours of the strain $e(x)$ for such cases as described in the last paragraphs are given in Fig. 2.

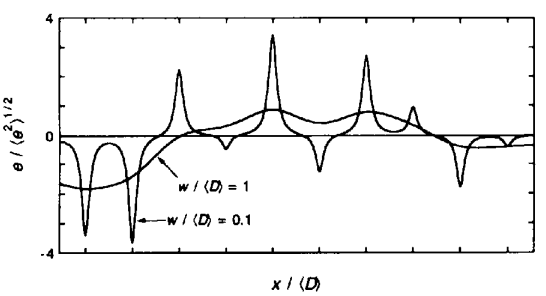

Fig. 2. Examples of the behaviour of the strain field $e(x)$ for two different values of the relative width $w/\langle D \rangle$ of the component strain fields using periodically distributed defects, a Gaussian $p_a(a)$ and a Lorentzian $f(x)$.

From Appendix *A*, it can be readily verified that, for any $p_a(a)$, $p_D(D)$ and $f(x)$, Fourier coefficients can be expressed in terms of dimensionless quantities exclusively; this is realized here by relating the parameters to the average projected-defect distance $\langle D \rangle$: $L_r \equiv L/\langle D \rangle$, $w_r \equiv w/\langle D \rangle$, $x_r \equiv x/\langle D \rangle$ and $d_r^* \equiv d^*\langle D \rangle$. This implies that line profiles of specimens with different $\langle D \rangle$ (all other things equal) have line widths proportional to $\langle D \rangle^{-1}$ and that they are identical if plotted on an $s_r = s\langle D \rangle$ scale.

Using periodically distributed projected defects, a Gaussian p_a and a Lorentzian $f(x)$, the Fourier cosine coefficients $A(L_r, d_r^*)$ can be written as [substitute L_r, x_r, d_r^* and (26) into (28) and substitute $x_i = i\langle D \rangle$ and L_r, w_r and x_r into (34)]:

$$A(L_r, d_r^*) = \int_{-1/2}^{1/2} \mathrm{d}x_r \exp\Bigg(-2\pi^2 d_r^{*2}\, 2w_r\langle e^2 \rangle/\pi \times \sum_{i=-\infty}^{\infty} \{\arctan[(x_r - i + L_r/2)/w_r] - \arctan[(x_r - i - L_r/2)/w_r]\}^2 \Bigg). \quad (7)$$

Use has been made of a simple relation between the mean-squared strain $\langle e^2 \rangle$ and $\langle a^2 \rangle$: $\langle e^2 \rangle = C\langle a^2 \rangle/\langle D \rangle$ [(32)] with C according to (29). Note that d_r^* and $\langle e^2 \rangle$ occur only in the combination $d_r^*\langle e^2 \rangle^{1/2}$; therefore, using $d_r^*\langle e^2 \rangle^{1/2}$ as a variable, the influence of both parameters is investigated at the same time.

Thus, the strain-field model for the specific case expressed by (7) describes diffraction-line broadening on the basis of three parameters: $\langle D \rangle$, $d_r^*\langle e^2 \rangle^{1/2}$ and w_r.

3. Order dependence of line broadening

In the following discussion of order dependence of line broadening, the parameters dealt with are the integral breadth and the Fourier coefficients of the line profiles, since these parameters are used in traditional methods of line-profile analysis.

The behaviour of the cosine Fourier coefficients $A(L_r, d_r^*)$ calculated using (7) is investigated as a function of the relative length of the diffraction vector $d_r^* = d^*\langle D \rangle$ (*i.e.* order of reflection). Since the profiles $I'(s_r, d_r^*)$ are symmetrical with respect to $s_r = 0$ [see second paragraph below (6)], their integral breadths $\beta_r(d_r^*) = \int I'(s_r, d_r^*)\,\mathrm{d}s_r/I'(0, d_r^*)$ [note that $\beta_r \equiv \beta\langle D \rangle$, where $\beta = \int I'(s, d^*)\,\mathrm{d}s/I'(0, d^*)$] are calculated here from the cosine Fourier coefficients according to

$$\beta_r(d_r^*) = \left[\int_{-\infty}^{\infty} A(L_r, d_r^*)\,\mathrm{d}L_r\right]^{-1} \quad (8)$$

The behaviour of $\beta_r(d_r^*)$ as a function of $d_r^*\langle e^2 \rangle^{1/2}$ and w_r is shown in Fig. 3. As expected, $\beta_r(d_r^*)$ increases

with increasing $d_r^* \langle e^2 \rangle^{1/2}$. The magnitude and rate of increase strongly depend on the relative width w_r of the strain fields of the individual defects. In the following, two extreme cases (infinitely broad and infinitely narrow component strain fields; see §3.1 and §3.2, respectively) are discussed; then, intermediate cases are considered (see §3.3).

3.1. *Infinitely broad component strain fields*

For $w_r \to \infty$, the breadth increases linearly with $d_r^* \langle e^2 \rangle^{1/2}$ (see Appendix *C* and Fig. 3*a*):

$$\beta_r(d_r^*) = (2\pi)^{1/2} d_r^* \langle e^2 \rangle^{1/2}. \tag{9}$$

This behaviour is well known for the strain broadening from specimens with a uniform lattice spacing d within each grain and a Gaussian spacing distribution over the grains, where $\langle e^2 \rangle = (\langle d^2 \rangle - \langle d \rangle^2)/\langle d \rangle^2$ (Stokes & Wilson, 1944). Note that (9) or its equivalent on a 2θ scale [$\beta = 2(2\pi)^{1/2} \langle e^2 \rangle^{1/2} \tan\theta$] has often been used for strain broadening *in general*.

The Fourier coefficients for $w_r \to \infty$ are given by (38). They are perfectly Gaussian and strongly order dependent: $\ln[A(L_r, d_r^*) = -(2\pi^2 \langle e^2 \rangle) L_r^2 d_r^{*2}$. The line shape of $I'(s_r)$ is also Gaussian. The shape, width and order dependence of $I'(s_r)$ are independent of the shape of $p_D(D)$, $p_a(a)$ and $f(x)$ (see Appendix *C*). An interpretation of part of the broadening considered here as order independent is out of order.

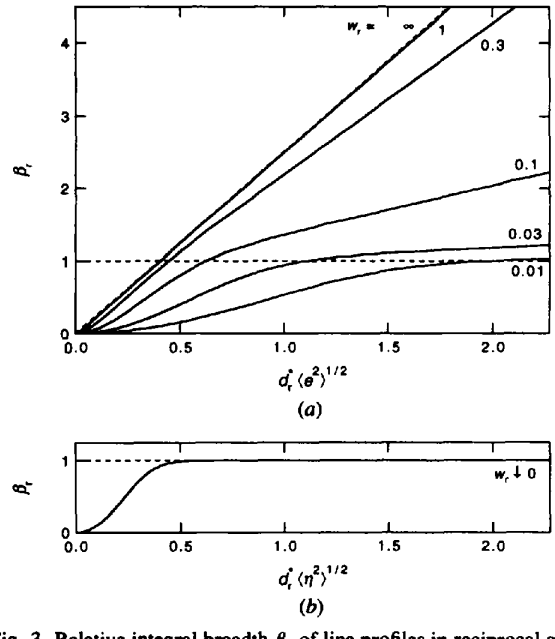

Fig. 3. Relative integral breadth β_r of line profiles in reciprocal space (*a*) as a function of $d_r^* \langle e^2 \rangle^{1/2}$ for different relative widths w_r of the component strain fields and (*b*) as a function of $d_r^* \langle \eta^2 \rangle^{1/2}$ (with $\langle \eta^2 \rangle = \pi w_r \langle e^2 \rangle$) for infinitely narrow component strain fields [$w_r \downarrow 0$; $\langle e^2 \rangle \to \infty$; see text below equation (10)] (dashed lines are asymptotes for $w_r \to \infty$ and $w_r \downarrow 0$).

3.2. *Infinitely narrow component strain fields*

In the limit $w_r \downarrow 0$, the relative integral breadth $\beta_r(d_r^*)$ reads [see (44) and Fig. 3(*b*)]

$$\beta_r(d_r^*) = [1 - \exp(-2\pi^2 d_r^{*2} \langle \eta^2 \rangle)] \times [1 + \exp(-2\pi^2 d_r^{*2} \langle \eta^2 \rangle)], \tag{10}$$

where the dimensionless parameter $\langle \eta^2 \rangle = \pi w_r \langle e^2 \rangle$ is used to characterize the strain content of infinitely narrow component strain fields (see Appendix *D*), recognizing that, in the limit $w_r \downarrow 0$, $\langle e^2 \rangle$ is an inconvenient parameter to measure the lattice distortions because there is only line broadening if $\langle e^2 \rangle$ is infinite (*cf.* Fig. 3*a*).

For small $d_r^* \langle \eta^2 \rangle^{1/2}$, it follows that $\beta \propto d^{*2}$. This case is related to the broadening observed from 'paracrystalline' materials (see discussion at the end of Appendix *D*). For larger $d_r^* \langle \eta^2 \rangle^{1/2}$, $\beta_r(d_r^*)$ approaches asymptotically to 1 [see (10) and Fig. 3]. For $d_r^* \langle \eta^2 \rangle^{1/2} \geq 1/2$, an increase of $\langle \eta^2 \rangle$ (strain content) or d_r^* (order of reflection) does not lead to an increase of the line breadth.

The Fourier coefficients and the corresponding line profile for $d_r^* \langle \eta^2 \rangle^{1/2} \geq 1/2$ approach [*cf.* (43) with $E = 0$]

$$A(L_r, d_r^*) = 1 - L_r \quad \text{for } L_r \leq 1; \quad \text{zero otherwise} \tag{11}$$

$$I'(s_r) \propto \sin^2(\pi s_r)/s_r^2. \tag{12}$$

Thus, the line broadening becomes completely independent of $\langle \eta^2 \rangle^{1/2}$ and d_r^*. Apparently, the line broadening from defects with larger strains confined to distances very much smaller than the average projected-defect distance is order independent. This type of strain broadening can be conceived as pure 'size broadening': small but undistorted crystals (here of size $\langle D \rangle$) induce exactly the same $I'(s_r)$ as the strained infinitely large crystal considered here (*e.g.* Delhez, de Keijser & Mittemeijer, 1982). If the defects are not periodically distributed, $A(L_r, d_r^*)$ and $I'(s_r)$ have more smoothly decaying tails but the same conclusions hold for the order dependence and the correspondence with pure size broadening (van Berkum *et al.*, 1996).

The model structure producing this type of broadening consists of blocks of undistorted material ('domains') shifted with respect to each other over distances $\langle D \rangle \eta_i$ [see (40)]. The phase differences corresponding with these shifts are $2\pi d_r^* \eta_i$ (modulo 2π). For $d_r^* \langle \eta^2 \rangle^{1/2} \geq 1/2$, these reduced phase differences are almost uniformly distributed over the reduced range of 2π in phase space. Thus, incoherency of diffraction can be understood for such $d_r^* \langle \eta^2 \rangle^{1/2}$ values (see §1). A practical example of such a structure is a specimen with small-angle boundaries with relatively high dislocation densities in the boundaries, in which the lattice distortion due to the dislocations in the boundaries is

large but confined to narrow regions adjacent to the boundaries [see results for large D/d of Wilkens (1979)].

3.3. *Component strain fields with intermediate widths*

For intermediate w_r, the dependence $\beta_r(d_r^*)$ on $d_r^*\langle e^2\rangle^{1/2}$ is complex (see Fig. 3*a*). For not too small $d_r^*\langle e^2\rangle^{1/2}$, $\beta_r(d_r^*)$ can be described by a straight line with, if extrapolated, a positive intercept of the ordinate. With increasing w_r, the slope increases from 0 to $(2\pi)^{1/2}$, whereas the intercept decreases from 1 to 0. For $w_r \geq 1$, the behaviour is almost as for $w_r \to \infty$. For $w_r \leq 0.01$, $\beta_r(d_r^*)$, at the larger values of $d_r^*\langle e^2\rangle^{1/2}$, behaves almost as in the limit $w_r \downarrow 0$ (*cf.* Fig. 3*b*).

The behaviour of the Fourier coefficients for three intermediate w_r values is shown in Fig. 4. The shapes of the curves change from Gaussian for large w_r (Fig. 4*a*) to more or less straight lines for small w_r (Fig. 4*c*). The tails of the corresponding line profiles become more pronounced with decreasing w_r. Here, always a horizontal tangent in $L_r = 0$ is observed because the calculations pertain to an infinitely long column (see Fig. 4*d*; Warren, 1969). For such a case, the curvature d^2A/dL^2 in $L = 0$ is proportional to $d^{*2}\langle e^2\rangle$ (Eastabrook & Wilson, 1952). Since $d_r^{*2}\langle e^2\rangle$, which is proportional to the first term in the Taylor-series expansion for $A(L_r, d_r^*)$, is the same for all sets of Fourier coefficients shown in Fig. 4(*d*), the initial curvature is independent of w_r. The next term in the expansion of $A(L_r, d_r^*)$ is of opposite sign and is proportional to L_r^4, $\langle e^4\rangle$ and the mean squared strain derivative $\langle e'^2\rangle$ (van Berkum *et al.*, 1994). Since $e(x)$ takes more extreme values and steeper peaks for decreasing w_r (see Fig. 2), both $\langle e^4\rangle$ and $\langle e'^2\rangle$ increase with decreasing w_r (see also Appendix *E*). Consequently, the smaller w_r, the smaller the L_r value of the inflexion point of $A(L_r, d_r^*)$.

The shapes of a first and a second order of reflection are markedly different (see Figs. 4*a–c*): in general, the tails of $A(L_r, d_r^*)$ for the higher order of reflection are more pronounced in a relative sense [*e.g.* relative to the width at $A(L_r, d_r^*) = 0.5$]. The tails of the corresponding line profiles are also more pronounced for the higher order of reflection. The differences in line width between a first and a second order of reflection are influence strongly by w_r. In general, the difference diminishes with decreasing w_r (see Figs. 4*a–c*). Since order dependence of line broadening can be related to incoherency of diffraction, this observation can be interpreted as a gradual loss of coherency of the diffraction with decreasing w_r. In the limit $w_r \downarrow 0$, incoherent diffraction by the blocks of undistorted material between the defects ('domains') is obtained, as discussed in §3.2.

The above conclusions pertaining to intermediate w_r values are most relevant for practice (*cf.* §6.2).

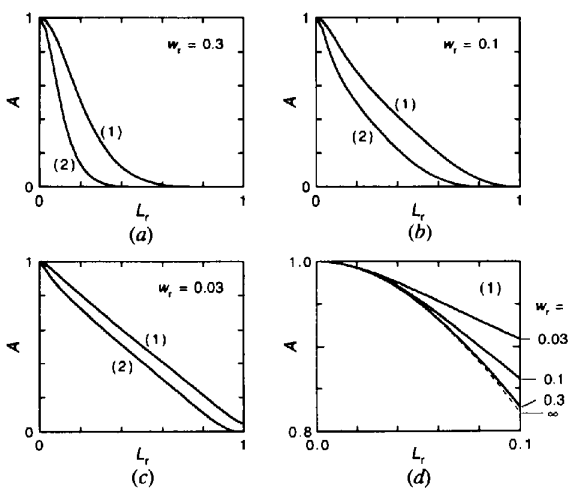

Fig. 4. Fourier coefficients of broadened line profiles calculated for three intermediate values (indicated) of the relative width w_r of the component strain fields: (*a*)–(*c*) using $d_r^*\langle e^2\rangle^{1/2} = 1$ [first order (1); upper line] and $d_r^*\langle e^2\rangle^{1/2} = 2$ [second order (2); lower line]; (*d*) behaviour at small L_r for first order ($d_r^*\langle e^2\rangle^{1/2} = 1$; dashed line is asymptote for $w_r \to \infty$).

4. Line-profile decomposition (size–strain separation) applied to simulated line profiles

Methods of analysis based on line-profile decomposition conceive the line profile $I'(s, d^*)$ as the convolution of an order-independent size-broadened profile $I'^S(s)$ and an order-dependent strain-broadened profile $I'^D(s, d^*)$. Usually, the characteristics of two (or more) line profiles $I'(s, d^*)$ with different values for the length d^* of the diffraction vector are used to estimate size and strain parameters that are intended to characterize the microstructure of the specimen.

In the following, line profiles calculated using (7) are analysed, in terms of size and strain parameters, as if they were real measurements, by means of the Williamson–Hall and the Warren–Averbach analyses.

4.1. *Williamson–Hall analysis*

4.1.1. *Procedure.* A number of methods use the integral breadths $\beta(d^*)$ (*i.e.* areas divided by heights) of line profiles $I'(s, d^*)$ to estimate the integral breadths β^S of $I'^S(s)$ and $\beta^D(d^*)$ of $I'^D(s, d^*)$ (for an overview, see Klug & Alexander, 1974). All these methods assume that $\beta^D(d^*) \propto d^*$ [*e.g.* $\beta^D(d^*) = (2\pi)^{1/2} e\, d^*$, where e is a strain parameter; *cf.* (9) and its discussion] and that $I'^S(s)$ and $I'^D(s, d^*)$ have specific shapes. These assumptions make them liable to systematic errors. Nevertheless, the methods are applied frequently and therefore one of them, the classical linear version of the Williamson–Hall plot, is investigated here.

In the linear version of the Williamson–Hall analysis (Williamson & Hall, 1953),† it is assumed that β^S and $\beta^D(d^*)$ are linearly additive. Further, β^S is identified with $(D_{WH})^{-1}$ and $\beta^D(d^*)$ is identified with $(2\pi)^{1/2}e_{WH}d^*$, where D_{WH} and e_{WH} are a size and a strain parameter, respectively. Therefore, a straight line is drawn through the data points in a plot of $\beta(d^*)$ *versus* d^* and the intercept of the ordinate is interpreted as $(D_{WH})^{-1}$ and the slope is interpreted as $(2\pi)^{1/2}e_{WH}$. If more than two orders of reflection are available and they do not lie on a straight line, the analysis should not be applied.

According to the present model, the behaviour of $\beta_r(d_r^*)$ as a function of $d_r^*\langle e^2\rangle^{1/2}$ is always more or less S shaped (see Fig. 3*a*). Consequently, the Williamson–Hall analysis should in fact not be applied. If the Williamson–Hall analysis is applied nevertheless, the slope and the intercept can take many different values dependent on the set of d_r^* employed (even negative intercepts are possible).

Only for relatively large $d_r^*\langle e^2\rangle^{1/2}$, say $d_r^*\langle e^2\rangle^{1/2} \geq 1/(10w_r)^{1/2}$, $\beta_r(d_r^*)$ follows a straight line (see Fig. 3*a*) and a Williamson–Hall analysis may be meaningful. To investigate the meaning of the parameters D_{WH} and e_{WH} in this case, $\beta_r(d_r^*)$ of a first and a second order of reflection have been calculated using $d_r^*\langle e^2\rangle^{1/2} = 1/(10\,w_r)^{1/2}$ for the first order (*e.g.* $d^* = 5\,\text{nm}^{-1}$, $\langle D\rangle = 40\,\text{nm}$, $w = 4\,\text{nm}$ and $\langle e^2\rangle = 25 \times 10^{-6}$, which appear reasonable values for cold-worked metals). From these $\beta_r(d_r^*)$ values, the size and strain parameters D_{WH} and e_{WH} have been deduced by means of the Williamson–Hall analysis. Since D_{WH} and e_{WH} refer to the size and the strain within independently diffracting 'domains' in the specimen and the line broadening is calculated from the strain field in an infinitely long coherently diffracting column, it is not self-evident what values of D_{WH} and e_{WH} should be expected. Rather arbitrarily, D_{WH} is compared with the average projected-defect distance $\langle D\rangle$ and e_{WH} with the root-mean-squared strain $\langle e^2\rangle^{1/2}$.

4.1.2. *Results and discussion.* The results obtained by means of the Williamson–Hall analysis as a function of w_r are shown in Fig. 5(*a*).

For very large w_r, all broadening is attributed to strain (*i.e.* $\beta^S = 0$ and $D_{WH} = \infty$), because $\beta_r(d_r^*) \propto d_r^*$ [see (9)]. The strain parameter e_{WH} equals $\langle e^2\rangle^{1/2}$. Thus, according to the Williamson–Hall analysis, a smoothly varying strain field induces pure strain broadening.

For $w_r \downarrow 0$, the Williamson–Hall analysis attributes all broadening to size (*i.e.* $\beta^D = 0$ and $e_{WH} = 0$) and D_{WH} equals $\langle D\rangle$. This is understandable too, since $d_r^*\langle e^2\rangle^{1/2} = 1/(10\,w_r)^{1/2}$ becomes very large for $w_r \downarrow 0$, in which case β_r approaches 1 and becomes independent of the order of reflection [see Fig. 3(*b*) for large $\langle\eta^2\rangle^{1/2}$]. Therefore, the line through the two calculated data points has zero slope and an intercept of the ordinate $\beta_r = 1$. Thus, in the Williamson–Hall analysis, the broadening due to a sharply peaked strain field is interpreted as pure size broadening, with a size parameter D_{WH} equal to the average projected-defect distance.

For intermediate w_r, the Williamson–Hall analysis attributes the calculated line broadening partly to size and partly to strain (see Fig. 5*a*). The size parameter D_{WH} is always larger than $\langle D\rangle$; the strain parameter e_{WH} is always smaller than $\langle e^2\rangle^{1/2}$. The deviations appear to be correlated: with increasing w_r the decrease of $\langle D\rangle/D_{WH}$ approximately equals the increase of $e_{WH}/\langle e^2\rangle^{1/2}$. However, the relation between the resulting values for D_{WH} and e_{WH} and the simulated strain field is unclear. In practice, without additional information on the nature of the strain field in the specimen,

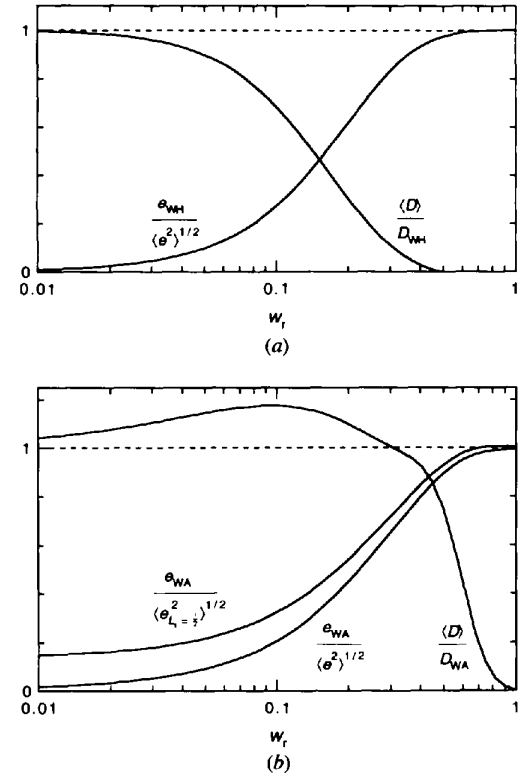

Fig. 5. Results of (*a*) the Williamson–Hall analysis and (*b*) the Warren–Averbach analysis as a function of the relative width w_r of the component strain fields. The analyses are applied to a first- and a second-order line profile, calculated using $d_r^*\langle e^2\rangle^{1/2} = 1/(10w_r)^{1/2}$ for the first order. The size parameters D_{WH} and D_{WA} are compared with the average projected-defect distance $\langle D\rangle$. The strain parameters e_{WH} and e_{WA} are compared with the root mean squared strain $\langle e^2\rangle^{1/2}$ and, in the case of e_{WA}, also with the true $\langle e^2_{L_r}\rangle^{1/2}$ at a relative correlation length $L_r = 1/2$ (for the definitions of the size and strain parameters, see text).

† On a 2θ scale, instead of on an s scale, the Williamson–Hall analysis involves a plot of $\beta\cos\theta$ *versus* $\sin\theta$. Then, the intercept of the ordinate is interpreted as λ/D_{WH} and the slope is interpreted as $2(2\pi)^{1/2}e_{WH}$.

D_{WH} can be anywhere between $\langle D\rangle$ and ∞ and e_{WH} between 0 and $\langle e^2\rangle^{1/2}$. The inappropriateness of Williamson–Hall analyses derives from assumptions regarding the integral breadths and shapes of the size- and strain-broadened profiles that do not hold in general.

4.2. *Warren–Averbach analysis*

4.2.1. *Procedure*. Several methods for line-profile decomposition use the Fourier coefficients $A(L, d^*)$ of two (or more) line profiles $I^I(s, d^*)$ to estimate, implicitly or explicitly, the Fourier coefficients $A^S(L)$ of $I^{IS}(s)$ and $A^D(L, d^*)$ of $I^{ID}(s, d^*)$ [note that $A^S(L)A^D(L, d^*) = A(L, d^*)$]. Since a set of Fourier coefficients represents a line profile in all its details, such Fourier methods can yield more detailed information on the microstructure than methods based on breadth parameters. A frequently applied Fourier method is the so-called Warren–Averbach analysis (Warren & Averbach, 1950, 1952).

In the Warren–Averbach analysis, it is assumed that $\ln[A^D(L, d^*)] = -2\pi^2L^2d^{*2}\langle e_L^2\rangle$ and consequently that $\ln[A(L, d^*)] = \ln[A^S(L)] - 2\pi^2L^2d^{*2}\langle e_L^2\rangle$, where $\langle e_L^2\rangle$ is the variance of e_L, the strain e averaged over a length L (see also Appendix *E*).† Therefore, a straight line is drawn through the data points in a plot of $\ln[A(L, d^*)]$ *versus* d^{*2} and the intercept of the ordinate is interpreted as $\ln[A^S(L)]$ and the slope is interpreted as $-2\pi^2L^2\langle e_L^2\rangle_{WA}$ (the subscript WA is added to $\langle e_L^2\rangle$ to distinguish the values obtained by means of the Warren–Averbach analysis from the true values). If L, d^* and the strains $e(x)$ are sufficiently small, the assumption used in the Warren–Averbach analysis is valid and the relation $\ln[A(L, d^*)]$ *versus* d^{*2} is linear. To determine if practical L, d^* and $e(x)$ values are small enough, the linearity of the relation is investigated below for Fourier coefficients calculated using (7). From $A^S(L)$ and $\langle e_L^2\rangle_{WA}$ for many L values, a size parameter $D_{WA} = \lim_{L\downarrow 0}[dA^S/dL]^{-1}$ and a strain parameter $e_{WA} = \lim_{L\downarrow 0}\langle e_L^2\rangle_{WA}^{1/2}$ can be calculated in principle. In practice, both limits for $L \downarrow 0$ cannot be determined reliably and one proceeds otherwise. To obtain a value of D_{WA}, usually a straight line is fitted to $A^S(L)$ in the L region where it has a reasonably straight portion and D_{WA} is taken as the L value at the intersection of the fitted line and the L axis. For a value of e_{WA}, the value of $\langle e_L^2\rangle_{WA}^{1/2}$ at $L = D_{WA}/2$ can be chosen (Klug & Alexander, 1974).

Next, regardless of the linearity, the Warren–Averbach analysis is applied here to Fourier coefficients of first- and second-order line profiles, calculated using the same w_r and $d_e^*\langle e^2\rangle^{1/2}$ as in §4.1. This size–strain separation yields $A^S(L)$ and $\langle e_L^2\rangle_{WA}$. Although the results of different practical procedures to calculate D_{WA} and e_{WA} (see above) deviate, in particular for D_{WA}, it was found that the trend and limiting cases discussed below are always the same. Here, for D_{WA}, a straight line is fitted to $A^S(L_r)$ for $1/3 < L_r < 2/3$ [this is the straightest part of $A^S(L_r)$ for all w_r]; for e_{WA}, the value of $\langle e_{L_r}^2\rangle_{WA}^{1/2}$ at $L_r = 1/2$ is taken. For the same reason as for D_{WH} and e_{WH} (see §4.1), it is not self-evident what values of D_{WA} and e_{WA} should be expected. As in §4.1, the estimate D_{WA} is compared with $\langle D\rangle$. For e_{WA}, the true $\langle e_{L_r}^2\rangle^{1/2}$ at $L_r = 1/2$ is used as reference.

4.2.2. *Results and discussion*. For practical values of L_r, d_r^* and $\langle e^2\rangle^{1/2}$, the linearity of the relation $\ln[A(L_r, d_r^*)$ *versus* d_r^{*2} strongly depends on the relative width w_r of the component strain fields (see Fig. 6). The true lines in Fig. 6 start in $A(L_r, d_r^*) = 1$ for $d_r^{*2}\langle e^2\rangle = 0$. Hence, for all values of L_r, a Warren–Averbach analysis for infinitely small $d_r^{*2}\langle e^2\rangle$ yields $A^S(L_r) = 1$ and $D_{WA} = \infty$, corresponding with the infinite column length considered here. For all L_r, the initial slope also yields exactly the true $\langle e_{L_r}^2\rangle$. However, due to the curvature of the true lines (explained briefly in Appendix *E*), straight lines through data points for practical $d_r^{*2}\langle e^2\rangle$ can yield intercepts deviating from zero and slopes deviating from $\langle e_{L_r}^2\rangle$ (see Figs. 6*b* and *c*).

For very large w_r (≥ 1), the true line remains straight up to large $d_r^{*2}\langle e^2\rangle$ and the straight line fitted in the Warren–Averbach analysis coincides with the true line (see Fig. 6*a*). Then the 'true' values are obtained (see Fig. 5*b*): $D_{WA} = \infty$ and $e_{WA} = \langle e_{L_r}^2\rangle^{1/2}$ at $L_r = 1/2$, which is almost equal to $\langle e^2\rangle^{1/2}$ in this case (*cf.* Fig. 11). Apparently, a smoothly varying strain $e(x)$ does not break up the column in 'domains'. The line broadening is interpreted as pure strain broadening.

For very small w_r (≤ 0.01), the true line is strongly curved at very small $d_r^{*2}\langle e^2\rangle$ and almost straight in the range where experimental data points are usually situated (see Fig. 6*c*). Since a straight line through the two data points coincides with a large portion of the true line, it appears a meaningful description of the behaviour of the Fourier coefficients, in spite of the deviation at very small $d_r^{*2}\langle e^2\rangle$. In §3 it was found that, for the case $w_r \downarrow 0$, the relatively little distorted regions between the 'walls of distortion' near the projected defects can be considered to scatter incoherently with respect to each other. This complies with the almost horizontal true line (see Fig. 6*c*): nearly pure size and little strain broadening. For $w_r \downarrow 0$, the size parameter D_{WA} tends to $\langle D\rangle$ and the strain parameter vanishes (see Fig. 5*b*).

For intermediate w_r values (~ 0.1), the true line does not have straight parts (see Fig. 6*b*). The straight line through the data points deviates from the true line in an arbitrary way. Different results would be obtained from

† The Warren–Averbach analysis can also be performed without taking the logarithm (Delhez & Mittemeijer, 1976). Advantages and drawbacks of both versions have been discussed by van Berkum *et al.* (1994).

different pairs of reflections (*cf.* Wilkens, 1979). Knowing the true line, one would not apply the Warren–Averbach analysis in such a case. If, however, as usual in practice, only two data points (*i.e.* two orders of reflection) are available and the curvature of the true line is unknown, the results of the Warren–Averbach analysis deviate from the 'true' values in an unknown way.

An example of the results of the Warren–Averbach analysis for intermediate w_r in terms of $A^S(L_r)$ and $\langle e^2_{L_r}\rangle_{WA}$ is shown in Fig. 7. The mean squared strains $\langle e^2_{L_r}\rangle_{WA}$ are much smaller than the true $\langle e^2_{L_r}\rangle$, except in the limit $L_r \downarrow 0$. The resulting behaviour of $A^S(L_r)$ is a problem in itself. It is curved downward for small L_r, which is in contradiction with the theoretical basis of the Warren–Averbach analysis. Truncation of the line profiles can cause such a 'hook effect' (Young, Gerdes & Wilson, 1967) but this effect is absent in the present calculations. Here, the hook effect is exclusively due to the violation of the assumption underlying the Warren–Averbach analysis. In the calculation of a size parameter D_{WA}, the theoretically correct method (using $\lim_{L\downarrow 0}[dA^S/dL]$) yields $D_{WA} = \infty$, which complies with the infinitely long column used in the calculations. In practice, however, a straight-line fit to some part of $A^S(L_r)$ is used, which yields $D_{WA}/\langle D\rangle$ values ranging from 0.6 to 1.2. Further, it follows from Fig. 5(*b*) that D_{WA} and e_{WA} depend strongly on w_r. As in the case of the Williamson–Hall analysis, it is concluded that, for intermediate w_r, the relation between the values determined for size–strain parameters, D_{WA} and e_{WA}, and the strain-field parameters is unclear. The inappropriateness of Warren–Averbach analyses derives from assumptions regarding the Fourier coefficients of the strain-broadened line profile that do not hold in general and from the arbitrariness of the estimate for D_{WA}.

5. Line-profile matching using the strain-field model

The observed limits of the fields of application of classical size–strain separation methods show the necessity for an alternative method for the analysis of line broadening from distorted specimens. Simulation and matching of line profiles on the basis of a strain-field model constitutes such a method. The model

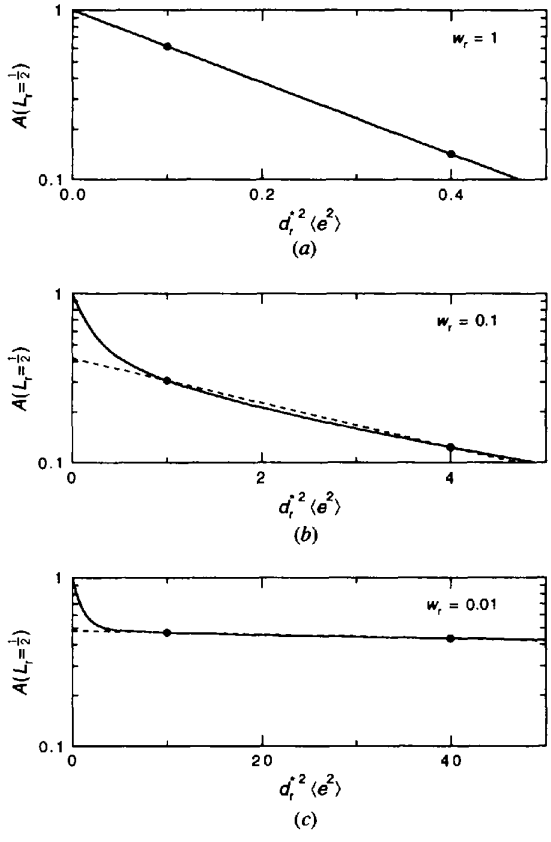

Fig. 6. Behaviour of $\ln[A(L_r, d_r^*)]$ as a function of $d_r^{*2}\langle e^2\rangle$ for a relative correlation length $L_r = 1/2$ and three relative widths w_r of the component strain fields: (*a*) $w_r = 1$, (*b*) $w_r = 0.1$ and (*c*) $w_r = 0.01$. The dots represent Fourier coefficients of a first and a second order of reflection with $d_r^*\langle e^2\rangle^{1/2} = 1/(10\,w_r)^{1/2}$ for the first order. In the Warren–Averbach analysis, the intercept of the ordinate and the slope of the dashed line are used to calculate size and strain parameters (for $w_r = 1$, the dashed line coincides with the full line).

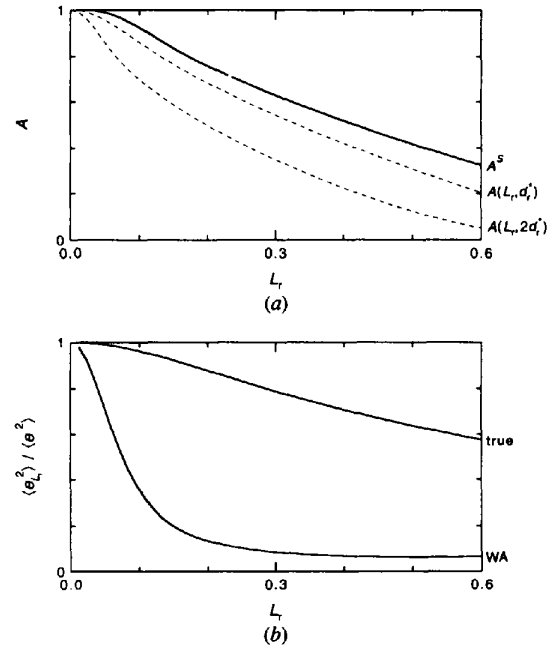

Fig. 7. Results of the Warren–Averbach analysis applied to Fourier coefficients $A(L_r, d_r^*)$ and $A(L_r, 2d_r^*)$ of a first- and a second-order line profile, respectively, calculated using $w_r = 0.1$ and $d_r^*\langle e^2\rangle^{1/2} = 1$ [$= 1/(10\,w_r)^{1/2}$] for the first order, in terms of (*a*) size coefficients $A^S(L_r)$ [$A(L_r, d_r^*)$ and $A(L_r, 2d_r^*)$ have been included for comparison] and (*b*) relative mean squared strains $\langle e^2_{L_r}\rangle_{WA}/\langle e^2\rangle$ [the true $\langle e^2_{L_r}\rangle/\langle e^2\rangle$ have been included for comparison].

parameters can be adapted and refined until certain characteristics of the simulated line profile fit certain characteristics of the measured one. The effect of instrumental line broadening, always present in measured line profiles, should either be removed from the measured line profile or added to the simulated line profile (see *e.g.* van Berkum *et al.*, 1992). If the fit succeeds, the model and the model parameters can provide a physically meaningful description of the strain field in the specimen.

The strain-field model presented in §2 can be used in a line-profile simulation and matching method. For this model, a single line-profile parameter, like the integral breadth $\beta(d^*)$, is usually not sufficient to determine the three model parameters $\langle D\rangle$, $\langle e^2\rangle^{1/2}$ and w_r. Fitting the full experimental line profile $I'(s)$ on the basis of (1) and (7) is laborious because each step in an iterative procedure involves a Fourier transformation. Therefore, fitting the Fourier coefficients $A(L, d^*)$ is advantageous. Equation (7) assumes, among other things, periodically distributed projected defects. For small and moderate L_r, the Fourier coefficients are not much affected by the distribution of projected defects along the column, but for large L_r they are (van Berkum *et al.*, 1996). Therefore, the fitting should be restricted to, say, $L_r \leq 1$ or a more general version of the strain-field model should be used.

If the average grain size $\langle T\rangle$ of the specimen is so small that it contributes to the observed line broadening, a factor $1 - L/\langle T\rangle$ (with $\langle T\rangle$ as a fixed or an adjustable parameter) can be added to the description of the Fourier coefficients to account for the grain-size broadening (only for $L \ll \langle T\rangle$).

The reliability of the results is very much enhanced if more than one line profile can be fitted simultaneously. In general, only orders of the same reflection can be used because the strain field may be systematically different in different crystallographic directions in the diffracting crystals. In the case of isotropic lattice distortion, all reflections of a deformed specimen can be used to determine a single set of model parameters (see *e.g.* §6).

In the next section, line-profile simulation and matching as a method of analysis (fitting Fourier coefficients calculated from a strain-field model to experimental ones) is investigated by applying the method to experimental line profiles.

6. Line-profile decomposition and line-profile matching applied to experimental line profiles

First, the acquisition and processing of the experimental data are described.

To obtain a sample of a cold-worked metal, a tungsten powder (>99.5 wt%, Fluka Chemika) was ball-milled for 1 h using two balls in a horizontally moving vessel. Tungsten was chosen because of its elastic isotropy. Ball milling was used because it is a many-sided ('isotropic') deformation procedure that is expected to produce dislocations with all possible combinations of Burgers' and line vectors. For these two reasons, the strain field in the specimen can be considered equivalent in all crystallographic directions and a simultaneous analysis of all measurable reflections is possible. Thus, the dependence of the integral breadth and the Fourier coefficients on the length of the diffraction vector can be studied with much more detail than in the case of an anisotropic material or an 'anisotropic' deformation procedure (using Cu $K\alpha$ radiation, eight reflections can be analysed for tungsten).

If the broadening effect of dislocations is to be investigated separately, other origins of line broadening should preferably be absent. The ball milling of tungsten produced some small particle fragments (see Fig. 8*a*), which would give rise to additional line broadening due to their finite sizes. These fragments were removed by a sedimentation procedure using 2-propanol. The average particle size after this treatment is definitely larger than 1 μm (see Fig. 8*b*). The line broadening due to such an average particle size is a negligible fraction of the total broadening.

A diffractometer specimen was prepared by suspending a small amount of the fractionated powder once more in 2-propanol and now sedimenting it onto a flat Si(510) single-crystal substrate. A silicon standard specimen, prepared according to van Berkum, Sprong, de Keijser, Delhez & Sonneveld (1995), was used to measure the instrumental broadening. Evidently, owing to the large difference in the absorption coefficients, silicon is an unsuitable standard material for a tungsten specimen in general. However, the transparency broadening by the Si standard specimen is decreased to a negligible level by using an Si layer thickness of *ca* 10 μm (Berkum *et al.*, 1995). Therefore, the Si standard specimen yields the correct

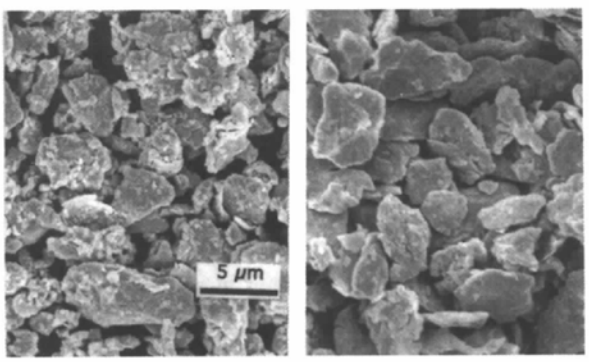

(*a*) (*b*)

Fig. 8. Scanning-electron-microscope observations of a ball-milled tungsten powder (*a*) before and (*b*) after removal of the smallest particles by means of sedimentation.

instrumental broadening for a practically non-transparent material like tungsten.

The X-ray diffraction-line profiles were recorded on a Siemens D500 diffractometer using Cu $K\alpha$ radiation and a graphite diffracted-beam monochromator. The divergence of the incident beam was 1° and the receiving-slit width was 0.05°2θ. The specimens were rotated around the normal to their surfaces during the measurements. For the tungsten specimen, the complete 2θ range (27 to 167°) was measured; for the silicon standard specimen, a sufficiently long range around each peak. For all profiles, linear backgrounds were subtracted and the Cu $K\alpha_2$ components were removed according to Delhez & Mittemeijer (1975). The profiles were then translated to intensity distributions $I'(s, d^*)$ in reciprocal space (with d^* corresponding to the centroid of I') and Fourier transformed. To obtain Fourier coefficients of the instrumental line profile for the d^* of the tungsten reflections, Fourier coefficients of the two nearest silicon reflections were interpolated linearly. Finally, the Fourier coefficients of the tungsten profiles were divided by those of the instrumental profiles to obtain the Fourier coefficients of the structurally broadened line profiles (Stokes, 1948).

The resulting sine coefficients were small for all reflections [$\sim 0.07A$ ($L = 0$) at most], indicating almost symmetrical line profiles. The integral breadths β can then be calculated from the Fourier coefficients using (8), Here, the range of integration (summation) was gradually increased and β was taken as the plateau value reached in a plot of the integral *versus* the range of integration. In this way, β of the structurally broadened line profiles was obtained without adopting a specific shape function.

6.1. *Line-profile decomposition using size and strain parameters*

The integral breadths of the eight reflections of the ball-milled tungsten powder plotted *versus* d^* lie reasonably on a straight line having a positive intercept with the ordinate (see Fig. 9*a*). The last two reflections show minor deviations from this line, which may be due to truncation effects (the 321 and 400 reflections probably have a little overlap and the 400 reflection is cut at $2\theta = 167°$). Exclusion of the last or last two reflections from the analysis does not alter the conclusions reached. Earlier measurements of integral breadths from tungsten filings yielded results very similar to Fig. 9(*a*) (Williamson & Hall, 1953; Langford, 1992). The size and strain parameters determined from Fig. 9(*a*) by means of the linear version of the Williamson–Hall analysis (see §4.1) are $D_{WH} = 62$ nm and $e_{WH} = 2.5 \times 10^{-3}$, *i.e.* the broadening is interpreted as partly due to size, partly due to strain, corresponding to an intermediate w_r value. Hence, according to §4.1, the Williamson–Hall size and strain parameters cannot be linked easily with the microstructure of the ball-milled powder.

The cosine Fourier coefficients of the experimental structurally broadened line profiles plotted logarithmically as a function of d^{*2} do *not* lie on a straight line (see Fig. 9*b*). A similar curvature can be observed in other recently published data obtained from ball-milled tungsten (Wagner, Yang & Boldrick, 1992). On the other hand, such curvature was not found by McKeehan & Warren (1953) and Aqua & Wagner (1964). The absence of such a curvature may be due to insufficient annealing of the standard specimen they used (see Williamson & Smallman, 1956). According to §4.2, when a Warren–Averbach analysis is applied to pairs of points (on the curved 'lines' of Fig. 9*b*), parameters are obtained that cannot be linked easily with the microstructure of the ball-milled powder. If it is performed nevertheless, the results depend on the reflections incorporated in the analysis. With the use of straight-line fits to all eight reflections (see Fig. 9*b*) and the practical procedures described in §4.2 to calculate D_{WA} and e_{WA}, the results are $D_{WA} = 17$ nm and $e_{WA} =$

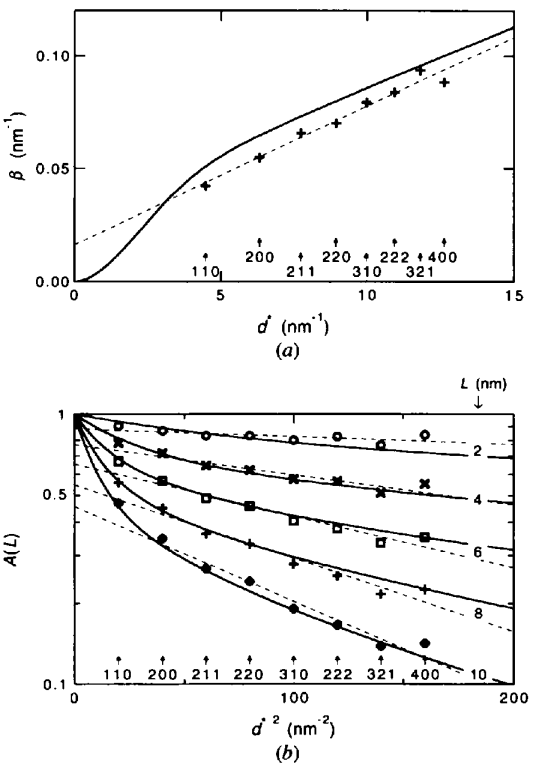

Fig. 9. Behaviours of (*a*) the integral breadth β as a function of d^* and (*b*) the logarithm of the Fourier coefficients $A(L)$ as a function of d^{*2} for the structurally broadened line profiles (*hkl* indicated at the bottom) of a ball-milled and fractionated tungsten powder. Dashed lines (straight-line fits to all eight data points) have been used in the Williamson–Hall analysis (*a*) and the Warren–Averbach analysis (*b*). Full lines have been calculated from the present strain-field model using $\langle D \rangle = 21$ nm, $w_r = 0.115$ and $\langle e^2 \rangle^{1/2} = 6.8 \times 10^{-3}$.

1.3×10^{-3}. The results using *e.g.* only 110 and 220 are $D_{WA} = 23$ nm and $e_{WA} = 2.2 \times 10^{-3}$. A (precarious) extrapolation of $\langle e_L^2 \rangle^{1/2}$ to $L = 0$ yields $\sim 3 \times 10^{-3}$ for all eight reflections and $\sim 5 \times 10^{-3}$ for only 110 and 220. Moreover, the $A^S(L)$ curves obtained always show a small 'hook effect'.

6.2. *Line-profile matching using the strain-field model*

Fourier coefficients calculated according to (7) and (8) have been fitted to the experimental Fourier coefficients of all eight reflections simultaneously (*cf.* §5). It was found that the parameter values $\langle D \rangle = 21$ nm, $w_r = 0.115$ and $\langle e^2 \rangle^{1/2} = 6.8 \times 10^{-3}$ yield the best fit (see the curved lines in Fig. 9*b*). These parameter values indicate that the strain along an arbitrary direction in the ball-milled powder shows significant peaks at average intervals of 21 nm, with a peak-width to peak-distance ratio of (on average) 0.115 [$w_r = w/\langle D \rangle$; see above (7)]. With the recognition that the data points for $L = 2$ nm are probably the least accurate owing to the unavoidable truncation of the measured profiles, the curved lines and the data points agree fairly well. This is remarkable considering the simplicity of the strain-field model used at present.

The behaviour of the integral breadth corresponding to the strain-field parameters estimated from the behaviour of the Fourier coefficients is indicated by the full line in Fig. 9(*a*). The discrepancy between the lines calculated using the model and the experimental data points in Figs. 9(*a*) and (*b*) is mainly ascribed to the periodic distribution of projected defects adopted in the model: it can be shown that non-periodic distributions yield Fourier coefficients that are comparable with the ones calculated here at small L, but that vanish more gradually at larger L (van Berkum *et al.*, 1996). Consequently, such distributions yield smaller β values [*cf.* (9)], with a better correspondence to the present experimental data.

From the parameter values obtained by fitting the Fourier coefficients, the results of the Williamson–Hall analysis and the Warren–Averbach analysis can be predicted: for $w_r = 0.115$, Fig. 5(*a*) yields $D_{WH} \simeq 1.6\langle D \rangle = 33$ nm and $e_{WH} \simeq 0.33\langle e^2 \rangle^{1/2} = 2.2 \times 10^{-3}$, and Fig. 5(*b*) yields $D_{WA} \simeq 0.85\langle D \rangle = 18$ nm and $e_{WA} \simeq 0.24\langle e^2 \rangle^{1/2} = 1.6 \times 10^{-3}$, in fair agreement with the results obtained in §6.2. The somewhat larger discrepancy for D_{WH} can be explained by the periodic projected-defect-distance distribution adopted (see above and *cf.* Fig. 9*a*).

The strain values obtained by means of line-profile decomposition (2.5×10^{-3} for e_{WH}; 3–5×10^{-3} for $\langle e_L^2 \rangle^{1/2}$ for $L \downarrow 0$) are significantly smaller than the root-mean-squared strain value obtained by means of line-profile simulation (6.8×10^{-3}). In the past, it has been observed that stored energies calculated from Warren–Averbach strains (stored energy is proportional to $\langle e^2 \rangle$) are smaller than those calculated from calorimetric measurements (Michell & Haig, 1957). The present results suggest that such discrepancies can be due to underestimation of the mean-squared strain by the Warren–Averbach analysis and that line-profile simulation and matching using the present model provides more accurate root-mean squared strain and stored-energy values.

7. Conclusions

The diffraction-line broadening due to lattice distortions associated with crystal defects can be described by means of a generally applicable model for the strain field in a column parallel to the diffraction vector. The strain-field model consists of a superposition of component strain fields, each of which is associated with a crystal defect close to the column, with statistically determined amplitudes and distances between the projections of the defects onto the column. In the present model, these amplitudes and distances are taken to be statistically independent. The average projected-defect distance $\langle D \rangle$, the width of the component strain fields relative to $\langle D \rangle$ and the mean-squared strain resulting from the superimposed component strain fields are the most important parameters in the model.

In the strain-field model, the average projected-defect distance $\langle D \rangle$ can be used as a scaling parameter The line width is proportional to $\langle D \rangle^{-1}$ and depends on the product of the root-mean-squared strain and the length of the diffraction vector (or the order of reflection). The width of the component strain fields relative to $\langle D \rangle$ strongly influences the (type of) order dependence of the line broadening and thereby the results of multiple-order line-profile decomposition methods, like the Williamson–Hall and the Warren–Averbach analyses.

For a smooth total strain field, *i.e.* for wide (relative to $\langle D \rangle$) component strain fields, the line broadening is strongly order dependent. This is interpreted by the Williamson–Hall and the Warren–Averbach analyses as pure strain broadening. For a strongly peaking strain field, *i.e.* for narrow (relative to $\langle D \rangle$) component strain fields and for a sufficiently large mean-squared strain, the line broadening is almost order independent. This is interpreted by the Williamson–Hall and the Warren–Averbach analyses as pure size broadening, with a size parameter equal to the average projected-defect distance $\langle D \rangle$. In all other cases, the order dependence is complex and the line-profile decomposition methods yield unclear results.

Matching line profiles calculated using a strain-field model to experimental line profiles provides a method of diffraction-line-broadening analysis that avoids *a priori* assumptions about the type of order dependence of the line broadening. Thereby, a more versatile approach to line-broadening analysis is possible.

The authors are grateful to Dr J. I. Langford for providing the tungsten powder and Ir A. Buis for providing scanning-electron-microscope facilities.

APPENDIX A
Fourier coefficients of a line profile for the strain-field model

According to (2) and (3), the Fourier coefficients $A(L, d^*)$ and $B(L, d^*)$ depend on the probability density $p_{Z_L}(Z_L)$, where Z_L is the elongation of a length L parallel to the column **x**. To find $p_{Z_L}(Z_L)$ for specific functions $p_D(D)$, $p_a(a)$ and $f(x)$, two equivalent procedures are possible. In the first procedure, a set $\{x_i\}$ of projected-defect positions x_i and a set $\{a_i\}$ of amplitudes a_i are generated from the functions $p_D(D)$ and $p_a(a)$, respectively, for a single infinitely long axis **x**. Then, Z_L is considered as a function of x along **x**, and the corresponding $p_{Z_L}(Z_L)$ is calculated from this $Z_L(x)$. In the second procedure, which is used in the following in a slightly modified [see below (15)] way, Z_L at a single arbitrary position x along **x** is considered for an infinite ensemble of axes, each with different sets of values $\{x_i\}$ and $\{a_i\}$. According to (4), (5) and (6), this $Z_L(\{x_i\}, \{a_i\})$ can be written as

$$Z_L(\{x_i\}, \{a_i\}) = \sum_{i=-\infty}^{\infty} Z_i, \tag{13}$$

where $Z_i = a_i F_L(x - x_i)$ and

$$F_L(x - x_i) = \int_{x-L/2}^{x+L/2} f(x' - x_i)\,dx' \tag{14}$$

(the order of summation and integration has been reversed). From this $Z_L(\{x_i\}, \{a_i\})$ at the position x, which is independent of x as long as **x** is infinitely long, $p_{Z_L}(Z_L)$ can be calculated. Since the set $\{x_i\}$ is statistically independent of the set $\{a_i\}$, it is allowed to calculate a probability density function $[p_{Z_L}(Z_L)]_{\{x_i\}}$ of Z_L for variable $\{a_i\}$ but fixed $\{x_i\}$ and to calculate the full probability density $p_{Z_L}(Z_L)$ from $[p_{Z_L}(Z_L)]_{\{x_i\}}$ by varying $\{x_i\}$. The latter procedure involves integration over all variables x_i accounting for the probability of specific sets $\{x_i\}$ by a probability density function $p_{\{x_i\}}(\{x_i\})$:

$$p_{Z_L}(Z_L) = \int \ldots \int p_{\{x_i\}}(\{x_i\})[p_{Z_L}(Z_L)]_{\{x_i\}} \prod_i dx_i. \tag{15}$$

For numerical calculations using (15), it is convenient to keep one of the defect positions fixed, say $x_0 = 0$, and vary only the set $\{x_i\}\backslash\{x_0\}$, *i.e.* all the variables x_i except x_0. This can be done only at the cost of additionally introducing a certain variation of the (initially fixed and arbitrary) position x. Thus, in (15), the integration over x_0 should be substituted by an integration over x. The range $(x_{-1}/2, x_1/2)$ is a sufficient variation of x because, for a certain set $\{x_i\}\backslash\{x_0\}$, each position x beyond this range [say $\frac{1}{2}(x_{\alpha-1} + x_\alpha) < x < \frac{1}{2}(x_\alpha + x_{\alpha+1})$, where α is a non-zero integer] is equivalent to (*i.e.* has surroundings identical to those of) the position $x - x_\alpha$ *within* the range $(\frac{1}{2}x'_{-1}, \frac{1}{2}x'_1)$ for the set $\{x'_i\}\backslash\{x'_0\}$, identical to the set $\{x_i\}\backslash\{x_0\}$ but translated along x over a distance x_α: $x'_i = x_{i+\alpha} - x_\alpha$. Since all possible sets $\{x_i\}\backslash\{x_0\}$ are considered, it is superfluous to extend the variation of x beyond the range $(x_{-1}/2, x_1/2)$. The probability density $p_{\{x_i\}\backslash\{x_0\}}(\{x_i\}\backslash\{x_0\})$ of the set $\{x_i\}\backslash\{x_0\}$, *i.e.* of the variables x_i in case $x_0 = 0$, follows from the independence of the variables $D_i = x_i - x_{i-1}$ and their probability densities:

$$\begin{aligned} p_{\{x_i\}\backslash\{x_0\}}(\{x_i\}\backslash\{x_0\}) &= \prod_i p_D(x_i - x_{i-1}) \\ &= \ldots p_D(-x_{-2} + x_{-1}) p_D(-x_{-1}) p_D(x_1) p_D(x_2 - x_1) \ldots . \end{aligned} \tag{16}$$

By substituting (16) into (15), excluding the integration over x_0 and integrating x over the indicated range, which has an average length equal to $\langle D \rangle$, one obtains

$$\begin{aligned} p_{Z_L}(Z_L) = (1/\langle D \rangle) &\int_0^\infty dx_1\, p_D(x_1) \int_{x_1}^\infty dx_2\, p_D(x_2 - x_1) \ldots \\ &\times \int_{-\infty}^{0} dx_{-1}\, p_D(-x_{-1}) \\ &\times \int_{-\infty}^{x_{-1}} dx_{-2}\, p_D(-x_{-2} + x_{-1}) \ldots \\ &\times \int_{x_{-1}/2}^{x_1/2} dx\, [p_{Z_L}(Z_L)]_{\{x_i\}}, \end{aligned} \tag{17}$$

where everything following a differential is the integrand of the corresponding integration. For the function $[p_{Z_L}(Z_L)]_{\{x_i\}}$, it is immaterial that now x and $\{x_i\}\backslash\{x_0\}$ are fixed instead of $\{x_i\}$.

Since all variables a_i are statistically independent, all terms Z_i in (13) are also statistically independent. Therefore, the probability density $[p_{Z_L}(Z_L)]_{\{x_i\}}$ of Z_L for fixed x and $\{x_i\}\backslash\{x_0\}$ but variable $\{a_i\}$ can be written as the convolution (denoted as $*$) of the probability density functions p_{Z_i} of the terms Z_i for all i:

$$\begin{aligned} [p_{Z_L}(Z_L)]_{\{x_i\}} = \ldots &* p_{Z_{-2}}(Z_L) * p_{Z_{-1}}(Z_L) * p_{Z_0}(Z_L) \\ &* p_{Z_1}(Z_L) * p_{Z_2}(Z_L) * \ldots , \end{aligned} \tag{18}$$

where, with the realization that $Z_i = F_L(x - x_i)a_i$,

$$p_{Z_i}(Z_L) = \big(p_a\{Z_L/F_L(x - x_i)\}\big)/[F_L(x - x_i)]. \tag{19}$$

If the function $f(x)$ decreases with increasing $|x|$, $F_L(x - x_i)$ decreases with increasing $|x - x_i|$ [see (14)], *i.e.*, for increasing $|i|$, if x is close to $x_0 = 0$. For decreasing $F_L(x - x_i)$, p_{Z_i} approaches a δ function [see (19)] and δ functions can simply be omitted in (18).

Therefore, only x_i and Z_i of defects with small $|i|$ have to be considered in (17) and (18).

After substitution of (17) into (2) and (3), the order of the integrations over x and $\{x_i\}\backslash\{x_0\}$ and the integration over Z_L can be reversed so that the resulting cosine Fourier coefficients can be written as

$$A(L, d^*) = (1/\langle D\rangle)\int_0^\infty \mathrm{d}x_1\, p_D(x_1)\int_{x_1}^\infty \mathrm{d}x_2\, p_D(x_2 - x_1)\ldots \times \int_{-\infty}^{0} \mathrm{d}x_{-1}\, p_D(-x_{-1}) \times \int_{-\infty}^{x_{-1}} \mathrm{d}x_{-2}\, p_D(-x_{-2} + x_{-1})\ldots \times \int_{x_{-1}/2}^{x_1/2} \mathrm{d}x\, [A(L, d^*)]_{\{x_i\}} \quad (20)$$

and the sine coefficients $B(L, d^*)$ can be related accordingly to $[B(L, d^*)]_{\{x_i\}}$, where $[A(L, d^*)]_{\{x_i\}}$ and $[B(L, d^*)]_{\{x_i\}}$ are Fourier coefficients for a specific x within $(x_{-1}/2, x_1/2)$ and a specific $\{x_i\}\backslash\{x_0\}$. These can be expressed in terms of the moments $\langle Z_L^n\rangle_{\{x_i\}}$ of $[p_{Z_L}(Z_L)]_{\{x_i\}}$ by a series expansion of the cosine and sine, respectively:

$$[A(L, d^*)]_{\{x_i\}} = \int_{-\infty}^{\infty} [p_{Z_L}(Z_L)]_{\{x_i\}} \cos(2\pi d^* Z_L)\,\mathrm{d}Z_L = 1 - (2\pi d^*)^2/2!\,\langle Z_L^2\rangle_{\{x_i\}} + (2\pi d^*)^4/4!\,\langle Z_L^4\rangle_{\{x_i\}} - \ldots \quad (21)$$

$$[B(L, d^*)]_{\{x_i\}} = \int_{-\infty}^{\infty} [p_{Z_L}(Z_L)]_{\{x_i\}} \sin(2\pi d^* Z_L)\,\mathrm{d}Z_L = -(2\pi d^*)^3/3!\,\langle Z_L^3\rangle_{\{x_i\}} + \ldots. \quad (22)$$

A term proportional to $\langle Z_L\rangle_{\{x_i\}}$ has been omitted in (22) because it is nil if $\langle a\rangle = 0$ [see below (18)]. From (13) and the independence of a_i and a_j for $i \neq j$, so that $\langle a_i^m a_j^n\rangle = \langle a_i^m\rangle\langle a_j^n\rangle$, the moments $\langle Z_L^n\rangle_{\{x_i\}}$ can be expressed in terms of the moments $\langle a^n\rangle$ of $p_a(a)$. Some examples are:

$$\langle Z_L^2\rangle_{\{x_i\}} = \langle a^2\rangle \sum_{i=-\infty}^{\infty} F_L^2(x - x_i) \quad (23)$$

$$\langle Z_L^3\rangle_{\{x_i\}} = \langle a^3\rangle \sum_{i=-\infty}^{\infty} F_L^3(x - x_i) \quad (24)$$

$$\langle Z_L^4\rangle_{\{x_i\}} = \langle a^4\rangle \sum_{i=-\infty}^{\infty} F_L^4(x - x_i) + 3\langle a^2\rangle^2 \times \sum_{i=-\infty}^{\infty}\sum_{j\neq 1} F_L^2(x - x_i)F_L^2(x - x_j). \quad (25)$$

By substitution of expressions like (23)–(25) into (21) and (22) and substitution of these into (20) and its analogue for $B(L, d^*)$ (only small $|i|$ are important), $A(L, d^*)$ and $B(L, d^*)$ can be calculated without evaluating the multiple convolution for $[p_{Z_L}(Z_L)]_{\{x_i\}}$ [*cf.* (18)]. Next, specific functions $p_a(a)$, $p_D(D)$ and $f(x)$ will be considered.

(i) *Probability density of strain amplitudes.* If $p_a(a)$ is taken symmetrical with respect to $a = 0$, then $\langle a^{2n+1}\rangle = 0$, $\langle Z_L^{2n+1}\rangle_{\{x_i\}} = 0$, $[B(L, d^*)]_{\{x_i\}} = 0$ [see (22)] and consequently $B(L, d^*) = 0$ so that the structurally broadened line profile is symmetrical. If $p_a(a)$ is taken Gaussian, the expression for $[A(L, d^*)]_{\{x_i\}}$ is also simplified significantly. In that case, $[p_{Z_L}(Z_L)]_{\{x_i\}}$ is a convolution of Gaussians [see (19)] and thus it is a Gaussian itself with a variance given by (23). Then, (21) reduces to (*cf.* Warren, 1959, p.152)

$$[A(L, d^*)]_{\{x_i\}} = \exp(-2\pi^2 d^{*2}\langle Z_L^2\rangle_{\{x_i\}}). \quad (26)$$

Note that, although a Gaussian $p_a(a)$ implies a Gaussian $[p_{Z_L}(Z_L)]_{\{x_i\}}$ (*i.e.* the probability density of Z_L *for a specific* x *within* $(x_{-1}/2, x_1/2)$ *and a specific* $\{x_i\}\backslash\{x_0\}$), $p_{Z_L}(Z_L)$ or $p_e(e)$, the probability density of the strain e, need not be Gaussian. The integrations over x and $\{x_i\}\backslash\{x_0\}$ can make the shape of $p_{Z_L}(Z_L)$ drastically different from that of $[p_{Z_L}(Z_L)]_{\{x_i\}}$. The shape of the full $p_{Z_L}(Z_L)$ depends on L and the functions $f(x)$, $p_D(D)$ and, of course, $p_a(a)$.

(ii) *Probability density of defect distances.* The simplest expression for $p_D(D)$ is a δ function at $D = \langle D\rangle$:

$$p_D(D) = \delta(D - \langle D\rangle), \quad (27)$$

which means that the defects are distributed perfectly regularly: $x_i = i\langle D\rangle$ ('periodically' distributed defects). In that case, (20) reduces to

$$A(L, d^*) = (1/\langle D\rangle)\int_{-\langle D\rangle/2}^{\langle D\rangle/2} [A(L, d^*)]_{\{x_i\}}\,\mathrm{d}x \quad (28)$$

with $x_i = i\langle D\rangle$ and the expression for $B(L, d^*)$ reduces accordingly.

(iii) *Shape of the component strain fields.* The shape and width of the strain fields of the individual lattice defects is represented by the function $f(x)$. The following normalization of $f(x)$ is used here:

$$\int_{-\infty}^{\infty} f^2(x)\,\mathrm{d}x = C, \quad (29)$$

where C is an arbitrary length constant [since $f(x)$ is dimensionless]. With such a normalization, the 'strain content' $\int e^2(x)\,\mathrm{d}x$ and consequently the stored elastic energy associated with a single defect in an infinitely long column is independent of the shape or width of $f(x)$. Next, it will be shown that, for the present model, a similar statement holds for a distribution of defects.

The mean-squared strain $\langle e^2\rangle$ for a distribution of defects in a column is calculated as follows. With (5) and (6) and the additivity of variances of independent variables, it follows for arbitrary $p_a(a)$ that

$$\langle e^2\rangle_{\{x_i\}} = \langle a^2\rangle \sum_{i=-\infty}^{\infty} f^2(x - x_i), \tag{30}$$

where $\langle e^2\rangle_{\{x_i\}}$ is the variance of e at x resulting from varying all a_i for fixed $\{x_i\}$. To obtain $\langle e^2\rangle$, $\{x_i\}$ is kept fixed to an arbitrary set of values and x is varied from $-\infty$ to ∞ [*cf.* the 'first' procedure below (14)]:

$$\langle e^2\rangle = \lim_{\Lambda\to\infty} (1/\Lambda) \int_{-\Lambda/2}^{\Lambda/2} \langle e^2\rangle_{\{x_i\}}\, dx, \tag{31}$$

where Λ is the averaging range in x. After substitution of (30) into (31) and reversal of the order of integration and summation, the terms $f^2(x - x_i)$ can be integrated separately. For $\Lambda \to \infty$, these integrations yield C [see (29)] for all defects. The number of such terms (= the number of defects in Λ) approaches $\Lambda/\langle D\rangle$ if $\Lambda \to \infty$ (law of large numbers). Thus, $\langle e^2\rangle$ is obtained as

$$\langle e^2\rangle = C\langle a^2\rangle/\langle D\rangle. \tag{32}$$

Hence, in the present model, the mean-squared strain and consequently the stored energy in the columns with arbitrary defect distributions are independent of the shape or width of the component strain fields. This is a consequence of the independence of the amplitudes of the component strain fields of adjacent projected defects.

If $f(x)$ has a Lorentzian shape (see §2.2 for discussion), it reads

$$f(x) = (2C/\pi w)^{1/2}[1 + (x/w)^2]^{-1}, \tag{33}$$

where w is the half-width at half-height of $f(x)$. Then, the integration according to (14) can be performed analytically and (23) can be written as

$$\langle Z_L^2\rangle_{\{x_i\}} = (2w\langle D\rangle\langle e^2\rangle/\pi) \times \sum_{i=-\infty}^{\infty} \{\arctan[(x - x_i + L/2)/w] - \arctan[(x - x_i - L/2)/w]\}^2, \tag{34}$$

where $C\langle a^2\rangle$ is eliminated using (32).

APPENDIX *B*
Strain fields round dislocations

Consider a straight screw dislocation in the z direction and through the origin of a rectangular coordinate system (x, y, z) in an infinite elastically isotropic medium. The only non-vanishing displacement component is u_z in the z direction (Hirth & Lothe, 1982):

$$u_z(x, y, z) = (b/2\pi)\arctan(y/x), \tag{35}$$

where b is the length of the Burgers vector. Consider an arbitrary line making an angle φ with the z direction and having its closest distance Δ to the z axis at the position (x_0, y_0, z_0), where $\Delta = (x_0^2 + y_0^2)^{1/2}$. Introduce a second rectangular coordinate system (x', y', z') with its origin at $(x, y, z) = (0, 0, z_0)$, the z' direction parallel to the line and the x' axis through $(x, y, z) = (x_0, y_0, z_0)$ (see Fig. 10). Then, the position $(x, y, z) = (x_0, y_0, z_0)$ becomes $(x', y', z') = (\Delta, 0, 0)$. The line is defined by $(x', y', z') = (\Delta, 0, p)$, where p is a variable. The coordinates (x, y, z) are related to (x', y', z') by

$$\begin{aligned} x &= x'\cos\theta - y'\sin\theta\cos\varphi - z'\sin\theta\sin\varphi \\ y &= x'\sin\theta + y'\cos\theta\cos\varphi + z'\cos\theta\sin\varphi \\ z &= z_0 - y'\sin\varphi + z'\cos\varphi, \end{aligned} \tag{36}$$

where $\theta = \arctan(x_0/y_0)$. In the z' direction, the displacement $u_{z'}$ equals $u_z\cos\varphi$. The strain in the z' direction $e_{z'z'}$ is identical to $\partial u_{z'}/\partial z'$. Expressing u_z according to (35) in terms of x', y' and z' using (36), $e_{z'z'}$ can now be calculated along the line (use $x' = \Delta$ and $y' = 0$):

$$e_{z'z'} = (b/2\pi\Delta)\{\cos\varphi\sin\varphi/[1 + (z'\sin\varphi/\Delta)^2]\}. \tag{37}$$

Thus, the strain along any line passing a screw dislocation behaves as a Lorentzian, with an amplitude and a width depending on the distance and the orientation of the line with respect to the dislocation line. For edge dislocations, the same procedure leads to the conclusion that only the tails of the strain profile along a line parallel to the Burgers vector behave as Lorentzian.

APPENDIX *C*
Infinitely broad component strain fields

If the strain fields of the individual defects are much broader than the average projected-defect distance ($w \gg \langle D\rangle$), the strain $e(x)$ consists of very many statistically independent contributions $e_i(x)$ [see (5) and (6)]. Therefore, the probability density $[p_e(e)]_{\{x_i\}}$ of e for arbitrary x and fixed $\{x_i\}$ (see 'second procedure' at the beginning of Appendix *A*) is Gaussian

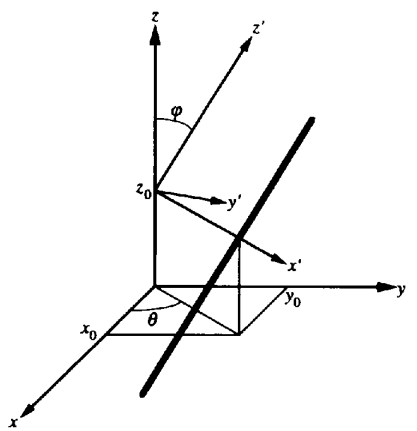

Fig. 10. The relation between two rectangular coordinate systems (x, y, z) and (x', y', z') and an arbitrary line (thick line) with its closest distance to the z axis at $(x, y, z) = (x_0, y_0, z_0)$.

(central limit theorem), independent of the shape of $p_a(a)$. The variance $\langle e^2\rangle_{\{x_i\}}$ is independent of $\{x_i\}$ owing to the large number of defects contributing to $e(x)$ if $w \gg \langle D\rangle$. Therefore, $\langle e^2\rangle_{\{x_i\}} \simeq \langle e^2\rangle$, independent of $p_D(D)$. Further, $e(x)$ is approximately constant over distances much smaller than w (*cf.* Fig. 2), so that $Z_L(x) \simeq Le(x)$ [see (4)] for $L \ll w$. In that case, $[p_{Z_L}(Z_L)]_{\{x_i\}}$ has the same shape as $[p_e(e)]_{\{x_i\}}$, which is Gaussian, and (26) is applicable, even if $p_a(a)$ is not Gaussian. The variance $\langle Z_L^2\rangle_{\{x_i\}} \simeq L^2\langle e^2\rangle_{\{x_i\}} \simeq L^2\langle e^2\rangle$ is also independent of $\{x_i\}$. Thus, in the limit $w/\langle D\rangle \to \infty$, (26) reduces to

$$A(L, d^*) = \exp(-2\pi^2 d^{*2} L^2 \langle e^2\rangle) \qquad \text{for } L \ll w. \quad (38)$$

If $w/\langle D\rangle = \infty$ and $\langle D\rangle$ is non-zero, $w = \infty$, so that the condition $L \ll w$ can be neglected. Then, the Fourier transform and, consequently, the corresponding line profile are Gaussian and the integral breadth can be calculated from (38) using (9):

$$\beta = (2\pi)^{1/2} d^* \langle e^2\rangle^{1/2}. \quad (39)$$

The above expressions hold for any shape $f(x)$ of the strain fields of the individual defects.

If $w/\langle D\rangle$ is large but finite, (38) holds approximately. If $d^*\langle e^2\rangle^{1/2} \geq 1/w$, $A(L, d^*)$ decreases virtually to zero for $L \ll w$ and the restriction $L \ll w$ can again be neglected. For smaller $d^*\langle e^2\rangle^{1/2}$, (38) is not an acceptable approximation for large L and β deviates from (39) (*cf.* Fig. 3 for $w/\langle D\rangle = 1$).

APPENDIX *D*
Infinitely narrow component strain fields†

In the limit $w/\langle D\rangle \downarrow 0$, the strain field of an individual projected defect is a δ function. Therefore, it is enclosed by the correlation length L completely or not at all. If L encloses projected defect i, then L is elongated by an amount $\langle D\rangle\eta_i$, where $\eta_i = Fa_i/\langle D\rangle$ with $F = \int f(x)\,dx$ [using (33) for $f(x)$, $F = (\pi wC)^{1/2}$]. In general, if m projected defects, numbered 1 to m, are enclosed in the interval $[x - L/2, x + L/2]$, then $Z_L(x)$ can be written as

$$Z_L(x) = \langle D\rangle \sum_{i=1}^{m} \eta_i. \quad (40)$$

The probability density of Z_L given that L encloses m defects is denoted as $[p_{Z_L}(Z_L)]_m$. If $p_a(a)$ is Gaussian with a variance $\langle a^2\rangle$, $[p_{Z_L}(Z_L)]_m$ is also Gaussian (all a_i are statistically independent) and it has a variance $m\langle D\rangle^2\langle\eta^2\rangle$, where $\langle\eta^2\rangle = F^2\langle a^2\rangle/\langle D\rangle^2$ [$= \pi w\langle e^2\rangle/\langle D\rangle$ if (33) is used for $f(x)$]. For fixed $\{x_i\}$, the interval $[x - L/2, x + L/2]$ encloses different numbers m of defects for different positions x. If the probability that L encloses m defects is denoted as $p_m(m)$, then $p_{Z_L}(Z_L)$ can be written as

$$p_{Z_L}(Z_L) = \sum_{m=0}^{\infty} p_m(m)[p_{Z_L}(Z_L)]_m. \quad (41)$$

Substituting (41) in (2) and solving the integral for each m separately yields

$$A(L, d^*) = \sum_{m=0}^{\infty} p_m(m)\exp(-2\pi^2 d^{*2} m\langle D\rangle^2\langle\eta^2\rangle) = \sum_{m=0}^{\infty} p_m(m)E^m, \quad (42)$$

where $E = \exp(-2\pi^2 d^{*2}\langle D\rangle^2\langle\eta^2\rangle)$.

In the case of a δ function for $p_D(D)$, *i.e.* projected defects are always separated by a distance $\langle D\rangle$, then a correlation length $L < \langle D\rangle$ encloses no projected defects with a probability $p_m(0) = (\langle D\rangle - L)/\langle D\rangle = 1 - L_r$ or one defect with a probability $p_m(1) = L/\langle D\rangle = L_r$; $p_m(m) = 0$ for $m > 1$. Generally, an arbitrary length L encloses M defects with a probability $p_m(M) = M + 1 - L_r$ or $M + 1$ defects with a probability $p_m(M + 1) = L_r - M$ where M is the integer part of L_r; all other $p_m(m)$ are nil. Calculating $A(L, d^*)$ using (42) and these $p_m(m)$ values yields

$$A(L, d^*) = (M + 1 - L_r)E^M + (L_r - M)E^{M+1}. \quad (43)$$

Note that $A(L, d^*)$ has a negative slope in $L = 0$ equal to $-(1 - E)/\langle D\rangle$, which is usually interpreted as indicating a 'domain size' equal to $\langle D\rangle/(1 - E)$ (*e.g.* Warren, 1969). This, for strain broadening, unrealistic feature occurs only for hypothetical infinitely narrow component strain fields; for all component strain fields with a finite width, $A(L, d^*)$ is horizontal and curved downwards for $L = 0$ (see Fig. 4 and its discussion in §3.3).

The relative integral breadth $\beta(d^*)$ of a line profile can be calculated from (43) using (9) by collecting the terms containing equal powers of E, yielding

$$\beta_r(d^*) = \{1/[2(1 + E + E^2 + \ldots) - 1]\} = (1 - E)/(1 + E). \quad (44)$$

For very small $d^*\langle D\rangle\langle\eta^2\rangle^{1/2}$ (*i.e.* $E \uparrow 1$), $\beta_r(d^*) \simeq \pi^2 d^{*2}\langle D\rangle^2\langle\eta^2\rangle$ (see, for E, below (42)]. The proportionality $\beta \propto d^{*2}$ has been derived theoretically and observed experimentally for the class of 'paracrystalline' materials (Kulshreshtha, Dweltz & Radhakrishnan, 1971). The ideal paracrystal can indeed be considered as a special case of the model presented in this paper: infinitely narrow component strain fields ($w/\langle D\rangle \downarrow 0$) with the average defect distance $\langle D\rangle$ equal to the average lattice spacing d. Since the root-mean-squared spacing deviation $d\langle\eta^2\rangle^{1/2}$ in such a structure is much smaller than the spacing d itself and d^{*-1} is usually a small multiple of d, the quantity $d^*\langle D\rangle\langle\eta^2\rangle^{1/2}$ is small (as required for the discussed quadratic

† For very narrow distortion fields, *i.e.* w of the order of the lattice spacing d, the use of a continuum model becomes questionable. However, it was shown that Fourier coefficients calculated from discrete lattice planes displaced according to the present strain-field model and from the continuum model itself are identical for L values equal to a multiple of d.

behaviour of β). The behaviour of $\beta_r(d^*)$ for large $d^*\langle D\rangle\langle\eta^2\rangle^{1/2}$ (*i.e.* $E \downarrow 0$) is discussed in §3.2.

APPENDIX *E*
Strain distributions

The results of the Warren–Averbach analysis, as discussed in §4.2, can also largely be understood from an investigation of the frequency distributions $p_L(e_L)$ of $e_L(x)$, the average of $e(x)$ in the interval $[x-L/2, x+L/2]$. The function $e_L(x)$ can be considered as $e(x)$ smoothed by a rectangular window of width L. Thus, the variance $\langle e_L^2\rangle$ decreases continuously† with increasing 'smoothing', *i.e.* increasing L. Because in the shape function of the strain fields of the individual projected defects x and w occur only in the combination x/w [see (33)] and the contributions of the individual defects to e_L are uncorrelated, the behaviours of $\langle e_L^2\rangle$ *versus* L for different w coincide if they are displayed as a function of L/w. In relative quantities, this statement holds for $\langle e_{L_r}^2\rangle$ *versus* L_r/w_r (see Fig. 11*a*). Thus, $\langle e_{L_r}^2\rangle$ *versus* L_r decreases faster for small w_r than for large w_r. This can be understood from the sharply peaked behaviour of $e(x_r)$ for small w_r, which is flattened by the smoothing much faster than the smooth $e(x_r)$ for large w_r.

The shape of $p_{L_r}(e_{L_r})$ can be characterized by the kurtosis k_{L_r}, here defined as $\langle e_{L_r}^4\rangle/\langle e_{L_r}^2\rangle^2$ (see Fig 11*b*). For $L_r \gg 1$, the strain $e_{L_r}(x)$ consists of many contributions of different defects of comparable magnitude. The contributions are statistically independent because the values a_i are drawn independently. Then, according to the central limit theorem (the distribution of the sum of many independent variables becomes Gaussian), the shape of $p_{L_r}(e_{L_r})$ has to become Gaussian for large L_r. For a Gaussian distribution, $k_{L_r} = 3$. Indeed, k_{L_r} decreases with increasing L_r to approximately 3 for $L_r \geq 1$ (see Fig. 11*b*). Further, k_{L_r} increases with decreasing w_r, in particular for small L_r, because the maximum values of $e_{L_r}(x)/\langle e_{L_r}^2\rangle^{1/2}$ become increasingly extreme with decreasing w_r (*cf.* Fig. 2), implying an increase of $\langle e_{L_r}^4\rangle$ with constant $\langle e_{L_r}^2\rangle^2$. The oscillations in Fig. 11(*b*) ($k_{L_r} = 3$ for integer values of L_r and slightly larger in between) originate from the adopted periodicity for the distribution of the projected-defect distances. For non-periodic distributions, k_{L_r} decreases more smoothly to 3.

If, for a specific L, the distribution $p_L(e_L)$ is Gaussian, the assumption used in the Warren–Averbach analysis (see §4.2) is correct for this L value (Warren, 1959) and the line in the Warren–Averbach plot is straight. For large w_r, $p_L(e_L)$ is always almost Gaussian and straight lines should be obtained, which agrees with Fig. 6(*a*). If $p_L(e_L)$ is non-Gaussian, the assumption in the Warren–Averbach analysis can still be justified if L and $\langle e^2\rangle$ are sufficiently small (Warren, 1959). Apparently, for $w_r = 0.1$ and $w_r = 0.01$, the values of L and $\langle e^2\rangle$ pertaining to Figs. 6(*b*) and (*c*) are not small enough in this sense, which results in curved lines.

Since the behaviour of $\langle e_L^2\rangle$ has been discussed extensively in the past, the $\langle e_L^2\rangle$ calculated here are confronted with some expressions in the literature. The horizontal tangent to $\langle e_L^2\rangle$ in $L = 0$ and the parabolic decay for small L, derived from infinitely large grains by Turunen, de Keijser, Delhez & van der Pers (1983), are both present in Fig 11(*a*). For $2.5 < L/w < 15$, the $\langle e_L^2\rangle$ values in Fig. 11(*a*) (note that $L/w = L_r/w_r$) are approximately proportional to $\ln(C/L)$, the behaviour derived for strains around dislocations for small but not too small L (Wilkens, 1970). For larger L, the behaviour of $\langle e_L^2\rangle$ depends strongly on the details of the spatial ordering of the defects. Since only one projected-defect-distance distribution is considered here (the periodic one), the present $\langle e_L^2\rangle$ behaviour for larger L is unique. Finally, for very large L, $\langle e_L^2\rangle$ is proportional to L^{-1} [the $\langle e_L^2\rangle$ according to equation (4.7) and the equation below equation (*A*.8) of Wilkens

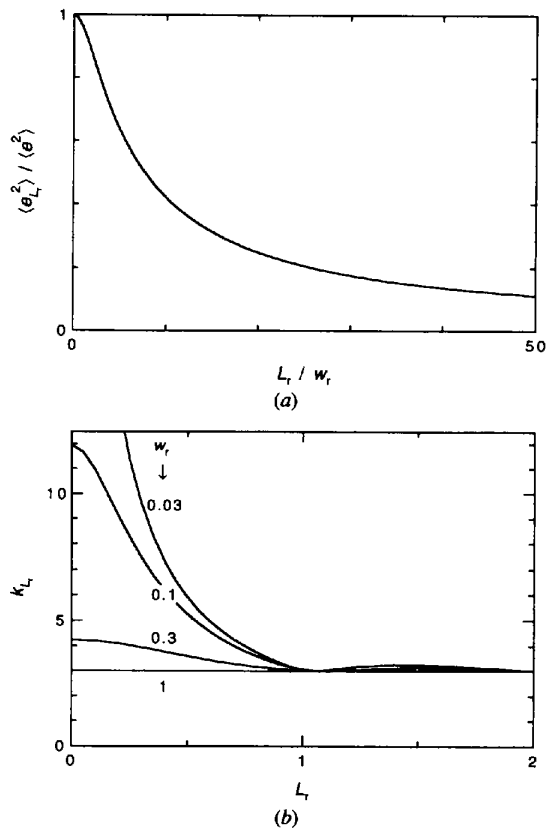

Fig. 11. Characteristics of the frequency distributions $p_{L_r}(e_{L_r})$ of e_{L_r}: (*a*) relative variance $\langle e_{L_r}^2\rangle/\langle e^2\rangle$ *versus* L_r/w_r and (*b*) kurtosis $k_{L_r} \equiv \langle e_{L_r}^4\rangle/\langle e_{L_r}^2\rangle^2$ *versus* L_r for different values of the relative width w_r of the component strain fields [if $p_{L_r}(e_{L_r})$ is Gaussian, then $k_{L_r} = 3$].

† This does not necessarily hold if the grains are small and enclose misfitting second-phase particles (*cf.* van Berkum *et al.*, 1992).

(1970) also show this behaviour]. This relation always holds for very large L because then the local strain $e_L(x)$ consists of *many* statistically independent contributions; a direct consequence is that $\ln[A(L, d^*)] \propto -L$ for very large L (Eastabrook & Wilson, 1952).

References

Aqua, E. N. & Wagner, C. N. J. (1964). *Philos. Mag.* **9**, 565–589.

Berkum. J. G. M. van, Delhez, R., de Keijser, Th. H. & Mittemeijer, E. J. (1992). *Phys. Status Solidi A*, **134**, 335–350.

Berkum, J. G. M. van, Delhez, R., de Keijser, Th. H. & Mittemeijer, E. J. (1996). *Proceedings EPDIC IV. Mater. Sci. Forum*. In the press.

Berkum, J. G. M. van, Sprong, G. J. M., de Keijser, Th. H., Delhez, R. & Sonneveld, E. J. (1995). *Powder Diffr.* **10**(2), 129–139.

Berkum, J. G. M. van, Vermeulen, A. C., Delhez, R., de Keijser, Th. H. & Mittemeijer, E. J. (1994). *J. Appl. Cryst.* **27**, 345–357.

Cowley, J. M. (1981). *Diffraction Physics*, pp. 73, 141. Amsterdam: Elsevier Science.

Delhez, R., de Keijser, Th. H. & Mittemeijer, E. J. (1982). *Fresenius Z. Anal. Chem.* **312**, 1–16.

Delhez, R. & Mittemeijer, E. J. (1975). *J. Appl. Cryst.* **8**, 609–611.

Delhez, R. & Mittemeijer, E. J. (1976). *J. Appl. Cryst.* **9**, 233–234.

Eastabrook, J. N. & Wilson, A. J. C. (1952). *Proc. Phys. Soc. London Sect. B*, **65**, 67–75.

Fowles, G. R. (1968). *Introduction to Modern Optics*, pp. 61–83. New York: Holt, Rinehart & Winston.

Hall, W. H. (1949). *Proc. Phys. Soc. London*, **62**, 741–743.

Hirth, J. P. & Lothe, J. (1982). *Theory of Dislocations*, 2nd ed, pp. 60, 78, 733. New York: John Wiley.

Klug, H. P. & Alexander, L. E. (1974). *X-ray Diffraction Procedures for Polycrystalline and Amorphous Materials*, pp. 661–665. New York: John Wiley.

Kulshreshtha, A. K., Dweltz, N. E. & Radhakrishnan, T. (1971). *J. Appl. Cryst.* **4**, 116–125.

Langford, J. I. (1992). *Accuracy in Powder Diffraction II*. NIST Special Publication No. 846, edited by E. Prince & J. K. Stalick, pp. 110–126. Washington: US Department of Commerce.

McKeehan, M. & Warren, B. E. (1953). *J. Appl. Phys.* **24**, 52–56.

Michell, D. & Haig, F. D. (1957). *Philos. Mag.* **2**, 15–32.

Sommerfeld, A. (1964). *Optics. Lectures on Theoretical Physics*, Vol. IV, pp. 191–193. New York: Academic Press.

Stokes, A. R. (1948). *Proc. Phys. Soc. London*, **61**, 382–391.

Stokes, A. R. & Wilson, A. J. C. (1944). *Proc. Phys. Soc. London*, **56**, 174–181.

Turunen, M, J., de Keijser, Th. H., Delhez, R. & van der Pers, N. M. (1983). *J. Appl. Cryst.* **16**, 176–182.

Wagner, C. N. J. (1966). *Local Atomic Arrangements*, edited by J. B. Cohen & J. E. Hilliard, pp. 219–269. New York: Gordon and Breach.

Wagner, C. N. J., Yang, E. & Boldrick, M. S. (1992). *Adv. X-ray Anal.* **35**, 585–592.

Warren, B. E. (1959). *Prog. Met. Phys.* **8**, 147–202.

Warren, B. E. (1969). *X-ray Diffraction*, pp. 264–268. Reading, MA: Addison-Wesley.

Warren, B. E. & Averbach, B. L. (1950). *J. Appl. Phys.* **21**, 595–599.

Warren, B. E. & Averbach, B. L. (1952). *J. Appl. Phys.* **23**, 497.

Wilkens, M. (1970). *Fundamental Aspects of Dislocation Theory*, NBS Special Publication No. 317, Vol. II, edited by J. A. Simmons, R. de Wit & R. Bullough, pp. 1195–1221. Washington: US Department of Commerce.

Wilkens, M. (1979). *J. Appl. Cryst.* **12**, 119–125.

Williamson, G. K. & Hall, W. H. (1953). *Acta Metall.* **1**, 22–31.

Williamson, G. K. & Smallman, R. E. (1956). *Philos. Mag.* **1**, 34–46.

Wilson, A. J. C. (1970). *Elements of X-ray Crystallography*, pp. 191–222. Reading, MA: Addison-Wesley.

Young, R. A., Gerdes, R. J. & Wilson, A. J. C. (1967). *Acta Cryst.* **22**, 155–162.